NASA TECHNICAL MEMORANDUM

NASA TM X-58017
March 1968

CONCEPT, DESIGN, AND PERFORMANCE OF THE MSC SPACECRAFT ACOUSTIC LABORATORY

By Robert J. Wren, Wade D. Dorland,
James D. Johnston, Jr., and Kenneth McK. Eldred
Manned Spacecraft Center
Houston, Texas

NATIONAL AERONAUTICS AND SPACE ADMINISTRATION

ABSTRACT

To obtain the best possible ground-test verification of the flight worthiness of the Apollo spacecraft to launch and boost fluctuating pressure environments, the NASA Manned Spacecraft Center conceived, designed, and constructed the Spacecraft Acoustic Laboratory, which embodies a unique vibratory simulation technique and capability. Apollo acoustic levels and spectra were used to develop acoustic test energy requirements and frequency considerations in the design of the sources, horns, and ducts. The test configuration includes 16 horn/duct channels, each driven by an independently controllable acoustic noise source, which completely envelop the vehicle and control the propagation of high-energy acoustic waves downward over the vehicle. Evaluation of the performance characteristics of the facility was oriented toward verification of acoustic test hardware design and, more importantly, toward comparison of Apollo vehicle vibration responses achieved in the ground test with flight measurements. With minor exceptions (which were corrected), all acoustic parameters designed into the hardware have been met or exceeded. The shell response of the service module as measured at eight locations during an Apollo flight has been duplicated satisfactorily in the laboratory.

CONTENTS

TABLE

FIGURES

CONCEPT, DESIGN, AND PERFORMANCE OF THE MSC SPACECRAFT ACOUSTIC LABORATORY

By Robert J. Wren, Wade D. Dorland,
James D. Johnston, Jr., and Kenneth McK. Eldred*
Manned Spacecraft Center

SUMMARY

The random fluctuating pressure (acoustic) excitation of the Apollo spacecraft during earth launch and boost is not only severe but also varies as a function of both flight mission time and location on the vehicle. To obtain the best possible verification of the flight worthiness of the spacecraft, evaluation was required of the vibration behavior of the Apollo spacecraft under severe acoustic conditions of flight in a ground test. A review of existing fluctuating-pressure simulation techniques and capabilities for full-scale spacecraft led to a concept, design, and development program which has produced an unusual simulation technique and capability. The evolution and embodiment of the simulation technique which resulted in the Spacecraft Acoustic Laboratory are described in this paper. Many simulation and facility hardware design problems were encountered, and both the problems and the solutions are discussed. Actual laboratory performance data are presented, and comparisons with flight measurements are made.

INTRODUCTION

The Apollo spacecraft (fig. 1) consists of the command module (CM), the service module (SM), and the lunar module (LM). During earth launch and boost, a rocket-propelled launch escape system (LES) is attached to the forward bulkhead of the CM, and a spacecraft lunar-module adapter (SLA) surrounds and protects the LM and also serves as the mechanical connection of the SM with the Saturn booster. In addition to the LES on the CM, many other aerodynamic protuberances, such as the reaction-control-system housing and nozzles on the SM, are located on the surface. The total acoustic excitation of the Apollo spacecraft during earth launch and boost reaches three peaks as a function of flight profile: (1) booster engine noise from the first stage of the Saturn at lift-off, (2) aerodynamic turbulence at transonic velocities, and (3) aerodynamic turbulence during maximum dynamic-pressure conditions at supersonic velocities.

---

*Director of Research, Wyle Laboratories, El Segundo, California.

The first acoustic peak can be described as a composite of progressive waves propagating from the base of the Saturn booster forward to the Apollo spacecraft. The second and third acoustic peaks represent the combined actions of several separate aerodynamic mechanisms which are either generated or intensified by the many vehicle protuberances projecting into the airstream and by abrupt changes in the vehicle mold line. These mechanisms include boundary-layer turbulence, separated flow, wake turbulence, and oscillating shocks. The varied nature of the acoustic loadings with respect to magnitude, spectral content, and correlation parameters dictated a ground test tool which would provide as much control over these parameters as possible. In addition, since the flight acoustic loadings are characterized by a spatial distribution of forces over the surface of the vehicle which is of a continuous nature (in lieu of several point forces, for example), a ground-test technique was required that would provide spatial continuity of the test forcing function.

During the concept studies in 1963 (ref. 1), the existing state of the art for simulation of launch and boost acoustic loading or other means of inducing flight-like vibration of spacecraft structures was surveyed and reviewed. The use of electromechanical or hydromechanical shakers, either singly or in multiples, was investigated. The potential use of acoustic waves led to the consideration of reverberation rooms, single-source progressive waves, and multiple-source progressive waves. A multiple-source, multiple-channel (or multiple-duct) approach was chosen with each source-channel to be acoustically separated from adjacent channels circumferentially around the vehicle. The sources were located forward of the vehicle to satisfy spatial profile requirements of the Apollo acoustic levels. The Apollo acoustic levels and spectra were used to develop acoustic test energy requirements and frequency considerations in the design of the sources and channels (horns and ducts). During the concept study, the selected approach was technically verified for practicality through the use of scale models.

The acoustic levels increased aftward on the CM (an uncommon condition since the acoustic levels decrease aftward on all other portions of the Apollo vehicle) which presented an unusually challenging acoustic test hardware design problem (ref. 2). The solution was found in the application of a technique using split horns with one horn reversed. The initial horn, reverse horn, and duct designs were verified with detailed scale models of the Apollo vehicle and of the acoustic test hardware.

The resulting test setup consists of 16 horn/duct channels each driven by an independently controllable acoustic-noise source. Each source is rated at 10 000 watts output. The channels completely envelop the vehicle and control the propagation of high-energy acoustic waves downward over the vehicle. The horns are constructed of fiber glass and steel, and the ducts and duct supports are constructed of wood and steel. Viscoelastic damping compound is used to reduce vibration of steel components. The ducts are adjustable inward or outward so that the cross section of the area through which the progressive waves propagate can be varied. Anechoic wedge terminators are used at the end of each wave propagation channel. Acoustic energy is produced by 16 pneumoacoustic sources, or air modulators. Air is supplied to these devices by a large constant-flow air compressor. Modulation of air valves in the devices is both controlled and powered by electrical control equipment located in a control room adjacent to the test area.

The acoustic hardware was checked out, evaluated, and adjusted during a step-by-step series of checkout test programs. The objective of each checkout experiment included simplicity of operations, with rapid feedback of results. The experiments proceeded in an orderly progression from single horns to multiple horns and from single Apollo modules to multiple modules; this was done for simplicity and to assure isolation of the hardware components and the dynamic parameters under evaluation. Potential physical interference of the ducts with the vibration response of the shells of test vehicles was investigated in a series of shaker tests. During these tests, the characteristic response was first measured at selected points on the bare checkout test article; then the vehicle response was measured at the same points after the horn/duct system had been mated with the test article.

Evaluation of the performance characteristics of the facility was oriented toward verification of acoustic test hardware design and, of more importance, toward comparison of Apollo vehicle vibration responses achieved in the ground test with flight measurements. With minor exceptions (which were subsequently corrected), all acoustic parameters designed into the hardware were met or exceeded.

Effects on the vehicle shell response of physical contact with the ducts are negligible. The SM shell-vibration data from the laboratory tests compare quite favorably with flight data. The shell response of the SLA as measured at three locations on two separate flights has been duplicated satisfactorily in the laboratory.

In this paper, the facility design requirements will be discussed first. The discussion will include the philosophy of environmental simulation, the sources of vibration in space vehicles during flight, the aerodynamic pressure fluctuations around the Apollo vehicle, and the simulation of such pressure fluctuations. The next section will describe the final facility design, including the test configuration and the equipment for the Apollo vehicle. Finally, the performance of the facility (for the Apollo configuration) is reported and analyzed. Comparisons are made between intended and actual performance.

FACILITY DESIGN REQUIREMENTS

Philosophy of Environmental Simulation

The purpose of the Apollo acoustic tests as established by the NASA Manned Spacecraft Center (MSC) was to evaluate probable spacecraft vehicle structure and equipment response, failure, or malfunction in the flight environment. Therefore, the criteria applied to the method of laboratory simulation were based on the need to reproduce probable flight responses.

To obtain the maximum information from the complete system test, it was deemed desirable to have the capability for all systems, including the astronauts, to be fully functioning during testing. To achieve this requirement, the vehicle axis had to be vertical so that the direction of the gravitational vector during flight would be duplicated for fuel tanks, personnel, et cetera.

Since the purpose of the tests was to produce responses similar to flight responses, the ideal test would have included (1) external pressure fluctuations with correct time and spatial relationships, (2) inertial forces (due to body acceleration of spacecraft/booster vehicles), (3) separation and ignition shocks, (4) engine vibration, (5) vibrations introduced via structural interfaces into upper stages (spacecraft) from lower stages (booster) that are associated with low-frequency body-bending modes of a complete spacecraft/booster vehicle, (6) external temperatures with time and spatial relationships, (7) quasi-static wind loads, and (8) external static pressure loads with time and spatial relationships. This is a most formidable list of environmental considerations; the simultaneous accomplishment, or even partial accomplishment, of which far exceeded the existing state of the art in 1963. Further, the concept of combined loadings was only beginning to be explored in the simultaneous application of two forcing functions. The acoustic laboratory was designed to allow accommodation simultaneously of all these loads except external temperatures and static pressures.

Accomplishment of acceleration and quasi-static loads is generally achieved by attaching tension members to various hard points on the vehicle (interstage rings, et cetera). The tension members can then transmit the forces of hydraulic jacks which may be programed. The facility structure was designed to enable installation of attach points for both vertical and horizontal load applications.

Accomplishment of shock, engine vibration, and interstage vibration would require placement of vibration generators at appropriate locations on the test vehicle, including the base of the stage under test. Exact simulation of structural interface impedance between stages is beyond the state of the art. However, the interface stiffness between the spacecraft and booster stages can be simulated. The assumption is made that structural impedances at the interfaces between spacecraft modules under test are simulated for all frequencies above the basic body resonances of the complete spacecraft/booster vehicle.

As previously implied, a major source of vibratory energy for the upper stages, including the spacecraft, is the external aerodynamically induced pressure fluctuations. The responses to these fluctuations depend on the pressure spectrum at a point, on the size of the area over which the pressures are correlated, and on the natural response characteristics of the structure. The size of the area is generally related to the scale of the turbulent phenomena causing the pressure fluctuations. Unfortunately, the area over which an acoustic wave is correlated, either in time or space, exceeds that over which the aerodynamic phenomena are correlated. Consequently, in many cases, the matching of an aerodynamic pressure spectrum at a point results in a greater generalized force on the vehicle structure. This effect is usually most apparent at low frequencies. Relationships between frequency, boundary-layer thickness, correlation, et cetera, have been obtained for the normal boundary layer, both experimentally and theoretically. However, no information was available which would give the space and time correlations for separated flow and oscillating shock phenomena.

Sources of Vibration in Spacecraft Vehicles During Flight

The four primary sources of spacecraft vibration (at frequencies above the basic body resonances of a complete spacecraft/booster vehicle) during flight are (1) vibrational energy transmitted from propulsion systems or other onboard machinery;

(2) vibration induced by ignition, stage separation, and docking impact transients; (3) vibration resulting from rocket noise impinging on the spacecraft shell during launch; and (4) vibration resulting from excitation of the spacecraft shell by aerodynamically derived external pressure fluctuations.

Motions associated with low-frequency body-bending modes of a complete spacecraft/booster vehicle usually are lower in level, and are not considered to be a primary source of high-level structural vibration, especially at high frequencies (above the basic body resonances of the complete spacecraft/booster vehicle).

In general, the vibration of propulsion systems dominates the vibration levels adjacent to the engines. However, little of the vibrational power is received by forward or remote areas of the spacecraft vehicle because of the attenuation within the damped structural path. This is especially the case for mechanical-borne vibration reaching the spacecraft from the propulsion engines of the lower booster stages.

Shock energy created by ignition, stage separation, and docking impact transients excites the fundamental vehicle vibratory modes and sometimes presents a very severe environment for structure and equipment mounted close to the source of the shock. However, little of the shock energy, particularly at the higher frequencies, is propagated to remote locations.

For much of a spacecraft vehicle, therefore, external pressure fluctuations, whether acoustic wave noise or aerodynamically induced, are responsible for the majority of internal vibration, structural fatigue failure, and equipment malfunction. Generally, the aerodynamic sources are more significant in the forward areas of a spacecraft vehicle, whereas the rocket-generated acoustic wave noise is dominant on the aft end. The simulation of fluctuating pressures associated with aerodynamic sources, or the structural vibration resulting thereof, is less straightforward than simulation of rocket-generated acoustic wave noise. Therefore, the characteristics of the aerodynamic environment will be discussed in detail in the next section.

Aerodynamic Pressure Fluctuations Around the Apollo Spacecraft Vehicle

The flow field around the Apollo spacecraft is rather complex (fig. 2) because of the many abrupt geometrical changes. The wake from the rocket tower of the LES covers the entire CM conical face during the launch phase. The presence of the wake makes it impossible for the bow shock, formed during supersonic flight in front of the blunt forebody (CM), to remain stationary. The abrupt transition at the shoulder of the CM creates a region of locally separated flow over the surface of the SM, which results in high-level excitation throughout the atmospheric portion of the flight. In addition, the entire SM is subjected to a forward-moving shock wave as the vehicle accelerates through the transonic region. Evidence of separated flow also exists over the SLA, and another flow separation occurs on the Saturn IVB (S-IVB) shoulder.

Several measurements of the surface pressure fluctuations have been made on models of typical spacecraft configurations (ref. 3). Numerous wind-tunnel tests using various scale models were also performed by North American Aviation, Inc., (NAA)

for NASA MSC at several wind-tunnel facilities, as noted in figure 3. (The latter data, although unpublished, were used for the Apollo Program environmental definition.) The maximum overall pressure-fluctuation levels for several typical stations around the Apollo vehicle at various Mach numbers are given in figure 3. The effect of the violent separation aft of the CM shoulder is clearly evident. The maximum overall level at this point, 173 dB (all fluctuating pressure and sound pressure levels are in decibels, referenced to 2×10^{-4} microbar), was obtained by NAA at the Douglas Aircraft Company, Inc., wind-tunnel facilities on a very small model. More controlled tests gave values of 166 to 168 dB. The average of all values was 169 dB.

Typical relative 1/3-octave band spectra in the shoulder area are given in figure 4. The results show a constant increase of 10 dB per decade from the lowest frequency to the spectral maximum in the vicinity of 80 Hz. This slope is independent of Mach number; however, the spectral levels above 80 Hz are influenced by Mach number with a considerable increase in the supersonic region. Absolute values of typical maximum spectra, without regard to Mach number or station, are given in figure 5. The peak in the vicinity of 80 Hz is well defined for all subsonic and transonic regions. The characteristic low-frequency slope of 10 dB per decade is also consistent, as is the tendency for the high-frequency noise to increase in supersonic flight.

The clear upper bound of the data in figure 5 and the similarity of the spectra enabled the selection of the design acoustic performance curve shown in figure 6. The design curve was selected to have an overall sound pressure level (SPL) of 171 dB at the shoulder position and to give a margin of 2 dB. The margin allowed for uncertainties (in the capabilities of the yet-to-be-developed noise-source system) and allowed for the possibility of attaining higher levels, if warranted, for specific test objectives.

The range of sound pressure spectra required to simulate the aerodynamically derived pressure spectra is shown in figure 7. The estimated spectrum from rocket noise at launch is also shown. Note that the aerodynamically derived pressure fluctuations are more severe than the rocket noise. The judgment was that achievement of the facility design spectra with appropriate levels at the various body stations would guarantee a test envelope which would be realistically conservative.

A method was required for simulating the fluctuating pressure field around the Apollo spacecraft where the test article was a 65-foot-high stack made up of the CM, SM, and SLA on a support fixture. The test article would be 13 feet in diameter at the SM and 22 feet in diameter at the base. Since the stack is a large item to test, a simulation technique would have to include consideration for the practical and economical methods of exciting such a specimen.

Simulation of the Pressure Fluctuations Around the Apollo Spacecraft Vehicle

Note that the use of shakers, either singly with excitation introduced at the base of the vehicle or in multiples with excitation introduced at several points on the vehicle surface, was discarded as an approach for simulation of the pressure fluctuations around the Apollo spacecraft vehicle. With single-input excitation at the base of the vehicle, the desired vibration field could not be achieved because of response attenuation, especially at higher frequencies, along the structural transmission paths to

points forward in the vehicle. A multiple-shaker approach would result in the more common problems encountered with this form of laboratory excitation tool when used for vibration testing of large vehicles. Some of these problems are that modifications would be required to the vehicle structure for attachment of shaker armatures; that vibration response in the vicinity of the shaker attachments would be excessive, which is unrealistic; and that control difficulties for a large matrix of shakers with inputs of random excitation would be formidable. For these reasons, further considerations emphasized acoustical input methods.

During the course of the conceptual development of the Spacecraft Acoustic Laboratory (SAL), three general methods of simulating the external pressure fluctuations by the use of acoustic wave impingement were proposed. These are illustrated in figure 8 and include (1) the reverberant field, (2) the progressive wave from either the bottom or the top of the test specimen, and (3) the multiple-source close-coupled progressive wave.

A reverberation-chamber approach offered considerable handling and placement flexibility for the Apollo and future spacecraft because few, if any, fixtures and ducts would be required. However, for the 270 000-cu-ft test tower required to enclose an Apollo vehicle configuration, the acoustic power requirements became rather large. For example, if the wall absorption coefficient were 0.03, the absorption would be 0.03 times 26 000 sq ft, which is 800 sabins. An input power of 2.5 million acoustic watts would be required to achieve an SPL of 170 dB in the chamber if the propagation in air were linear; however, because of macrosonic attenuation, the acoustic power requirement more probably would be on the order of 5 to 7 million acoustic watts. This power requirement would have far exceeded the most ambitious of previous facilities, and its cost would have been prohibitive.

More important, technically, the high-level sound field would surround the entire vehicle, including all sections which have much lower maximum flight levels. This would provide a quite unrealistic simulation, especially for the aerodynamic cases, and would cause much higher response of equipment and structures than occur in flight. Consequently, failures and malfunctions which might be experienced during the test would have a low probability of occurring in flight, thus potentially leading to an excessive number of structural fixes, overdesign, and overweight.

While high-level reverberant testing was impractical, it was desirable to be able to utilize the tower as a reverberation chamber at lower levels. This utilization would allow for future reverberant tests of large equipment and comparison of the responses of vehicle structure to two different types of test environment, reverberant and progressive wave acoustic excitation. For this purpose, the internal tower dimensions were selected as 90 feet high, 50 feet deep, and 61 feet wide to optimize the frequency separation of the acoustic modes in the chamber. In the optimization process, a height of 90 feet was selected to accommodate the vehicle, and a width of 50 feet was selected for architectural compatibility and for test-article handling space. The chamber modes were then calculated for a range of lengths between 54 and 65 feet in increments of approximately 1 foot. The 61-foot dimension provided the best results with good frequency response obtained above approximately 3.3 times the fundamental chamber resonant frequency of 6.2 Hz (approximately 20 Hz). Hence, good diffuse field characteristics were obtained for the entire frequency range of interest between 20 and 2500 Hz. Because of later additional architectural considerations, the basic

tower dimensions were increased to 101 feet high, 56 feet deep, and 68 feet wide, each dimension being adjusted by the same factor to maintain the optimum dimension ratios.

Two alternative methods of progressive wave testing using a duct-containment system were considered and are illustrated in figure 8. Both methods required approximately 160 000 acoustic watts of power to achieve 171 dB in a 3-inch-wide annular area around the command and service module (CSM) shoulder. Both concepts allowed simulation of the SPL gradient aft of the CSM shoulder by a combination of attenuation and increase in area function. Both could be terminated in similar manner, either alongside the SLA or around a portion of a simulated S-IVB stage.

A major difference in concept was the provision of multiple-source units. In the multiple-source configuration which was adopted, 16 sources would be utilized to drive 16 longitudinal ducts in lieu of one or two sources driving a single duct. Each of the 16 sources could be driven from an independent random-noise generator which would enable limiting circumferential correlation to a duct width of 30 inches, thereby improving the simulation flexibility.

A second major difference was the use of a folded horn rather than a direct horn for the CM. The principal difficulty with the direct horn was the requirement that the SPL at the nose be less than that at the shoulder. Consequently, the duct cross-sectional area would have to be greater at the nose than at the shoulder with the anticipation that this area expansion followed by a contraction and then an expansion would lead to considerable acoustic-transmission difficulties. The folded horn avoided some of the difficulties since its horn area expansion nearly matched the areas required to achieve the desired sound pressure levels. However, impedance discontinuities would occur at the throat of the folded horn. These discontinuities were minimized during the model portion of the concept study.

During the design phase, the mold lines for the horns and ducts were defined in detail. An opportunity to add, at little additional cost, the capability to drive the laboratory reverberantly with the 16 noise sources also became apparent in the design phase. This second mode of testing would be achieved by removing the ducts from the horns at the CSM shoulder and replacing them with 16 large horn flare sections. The flare sections would couple the noise sources to the room volume by using a portion of the test vehicle as the horn walls. The resulting acoustical conditions would retain progressive wave excitation over the surface of the CM and the upper surface of the SM. The lower surface of the SM and the surface of the SLA would be subjected to reverberant energy, thus affording versatility of the testing approach and an opportunity to compare the response of vehicles to both types of laboratory forcing functions.

The primary purpose of the SAL, as in any ground-based experimental facility, is to provide a tool which can be used to simulate one or more of the inservice environments of a spacecraft. With this tool, the experimenter may study the vibrations of either a full-scale or model vehicle to simulated environments, and then utilize the experimental results to predict the vibrations of the full-scale vehicle to actual environments. The utility of any experiment involving such simulation is proportional to the degree of confidence which can be placed in the accuracy of the vibration response predictions that can be made from the experiment. Under the proper choice of field parameters, different fluctuating pressure fields can produce essentially identical

average vibration response in a structure. Thus, in general, the simulated environment need not always be completely accurate in itself but rather must provide an accurate vibration prediction tool. The variable parameters for optimizing simulation, which served as design requirements for the SAL, are compared with flight conditions in table I.

The comparisons in table I indicate that the SAL could achieve a rather accurate simulation of the pressure field from rocket noise at launch and a less accurate simulation of the pressure field resulting from aerodynamic pressure fluctuations. The principal deficiencies of the latter simulation are (1) inability to simulate the longitudinal and lateral correlation functions except to the approximation of (sin ky)/ky, where k is the acoustic wavelength constant and y is distance, for the reverberant configuration; or cos ky, longitudinally, and one-sixteenth of the circumference laterally in the progressive wave patterns; and (2) inability to vary the spectrum as a function of longitudinal position in either configuration. These deficiencies result from the use of an acoustic field to simulate nonacoustic phenomena. However, the significance of the deficiencies is still not established. Existing theory and experience indicated that their effects could be minimized through development of proper equivalent spectra for the ground simulation. Therefore, early experimental programs in the SAL, together with supporting theoretical studies (refs. 4 and 5), were directed toward developing the necessary equivalences and proving the results by comparing the vibration field in actual vehicles measured both in flight and in the SAL. These efforts are continuing, and the results already achieved (ref. 6) toward simulation of flight response are quite promising. The following section is a detailed description of the facility, as built.

FACILITY DESCRIPTION

General

The SAL (fig. 9) is housed in a tower which has external dimensions of 105 feet high, 60 feet deep, and 70 feet wide. The tower consists of a structural steel framework with concrete panels for the exterior walls, and can accommodate a vehicle up to 30 feet in diameter and 85 feet in height. A door 40 feet high and 32 feet wide provides access for bringing individual spacecraft modules into the laboratory. The laboratory is serviced by a 75-ton fixed-point hoist which is used for stacking modular components of an integrated spacecraft, and which can be used to suspend a spacecraft during testing. A 5-ton circular bridge crane is used for general-purpose material handling and for handling test ducts. Permanent and movable platforms are located at elevations of 15, 30, 45, 60, and 75 feet. The movable platforms are 3-foot-wide catwalks which encircle the test vehicles. An elevator 6 feet wide, 7 feet deep, and 8 feet high is used for personnel and equipment access to the various levels and to the adjacent control room. Pneumatic and electrical utility connections, communications stations, and instrumentation and cable chases are located throughout the laboratory.

Two modes of testing are presently available in the laboratory: progressive wave, the primary mode; and progressive wave/reverberant fill-in, the secondary mode.

In progressive wave tests, the exposed surface of a test vehicle is enveloped by controlled high-intensity sound. Sixteen separate progressive wave sound fields are directed downward over the vehicle in separate encircling ducts as shown in figure 9. The cross-sectional area of the ducts is adjustable so that specified sound pressure levels can be achieved along the longitudinal axis of the test vehicle. Sound energy is supplied by 16 noise sources, or air modulators, which are electrically programed and have an output of 10 000 acoustic watts each. The air modulators are suspended from the top platform in the tower and are attached to coupling horns which are connected to the ducts. The air modulators are independently controlled so that the correlation of the acoustic fields between the ducts can be programed. The 160 000 acoustic watts of power generated by the air modulators provide an overall SPL of 169 dB at the horn/duct interface.

In progressive wave/reverberant fill-in testing, the ducts are removed from the horns and replaced with extension horn flare sections which couple the acoustic energy to the acoustic response modes of chamber volume. Thus, the lower portion of the vehicle is subjected to reverberant loading.

The air modulators require a large volume of compressed air (approximately 27 000 standard cu ft/min) which is supplied by a constant-flow centrifugal air compressor driven by a 4500-horsepower electric motor. The compressor is located in an adjacent building and draws its supply of air from within the tower, making the air system a closed loop, with the tower volume serving as a plenum. Air manifolds are connected to the air modulators by hoses.

Apollo Test Configuration

The SAL horn/duct system is presently configured specifically for the Apollo spacecraft (fig. 10). In this configuration, the complete Apollo test article (consisting of a CM, an SM, an SLA, and an LM located inside the SLA) is positioned on top of a Saturn instrument unit (IU) and a base fixture (which simulates the S-IVB forward skirt). The entire stack is in a vertical orientation. The dome of a forward tank of the S-IVB booster is also mounted, consistent with flight location, inside the S-IVB forward skirt to assure proper internal acoustical boundary conditions.[1] The circular duct system is positioned around the entire Apollo vehicle stack (fig. 11) to contain the high-energy acoustic progressive waves which are generated above the stack and passed aftward over the outer shells of the vehicles. Approximately 75 percent of the acoustic energy passes down over the SM. The remainder is directed via a splitter arrangement in the initial, or transition, horn section through a reverse, or folded, horn backup over the face of the CM. Anechoic termination wedges are located at the

---

[1] Standard longitudinal Apollo station numbers are used to identify measurement locations. These station numbers along the longitudinal axis are identified as X_a---- (with up to four digits to fill the blanks). In SAL, measurement locations from X_a 552 (bottom of the SLA) to X_a 1260 (top of the upper terminator) are available.

end of each duct run and of each horn run to assure that a plane wave condition is maintained. This is necessary to preclude the occurrence of standing acoustic waves and to assure compliance with plane wave propagation objectives. The latter allows the SPL to be increased or decreased along the length of the specimen by moving the outer wall of the duct in or out with respect to the vehicle outer shell (that is, the depth of the duct is variable). The spectral shape of the acoustic waves is controlled by appropriate programing of the electrical input signal to the driver coil of the air modulator which generates the acoustic waves. The acoustic levels are controlled by the programed output of the air modulator and by the radial placement of the duct with respect to the outer face of the vehicle shell. The duct is divided into 16 acoustically separate channels so that many combinations of levels, shapes, and correlations can be programed around the circumference of the test article.

The transition horns (fig. 12), which couple the air-modulator acoustic output with the folded-horn/duct system, are constructed of epoxy fiber glass and have access ports for mounting microphones so that the microphone diaphragms are flush with the internal wall of the horns. The transition horns are bolted to the steel folded-horn sections which surround the CM. A steel upper terminator unit having 16 compartments, each lined abundantly with fiber-glass absorptive material and fitted with fiber-glass wedges, is bolted to the top of the 16 folded-horn sections. The V-shaped duct supports (fig. 13), which are bolted to the lower faces of the folded-horn sections and extend downward over the SM, SLA, and IU, are constructed of plywood faced with sheet metal. The outer walls of the ducts (fig. 14) are steel rolled to a curvature that is concentric with the surface of the test article. Slotted tabs are provided on the outer walls of the ducts, and multiple bolting locations are provided on the V-shaped duct supports to allow radial adjustment of the cross-sectional area of the ducts. The cross-sectional area of each duct is bounded by the outer wall, two walls of the V-shaped duct supports, and the surface of the test vehicle. In a similar fashion, the surface of the CM serves as a fourth horn boundary in the reverse-horn sections. Fiber-glass wedges, which serve as lower terminators, are positioned at the bottom of each duct in the area of the IU and the base fixture. When the reverberant flare system (fig. 15) is used in lieu of the duct system, the acoustic progressive waves are coupled directly to the room and no anechoic terminators are used. All steel walls of the horn/duct assemblies are coated with several thick layers of viscoelastic damping compound. The weight of the horn/duct assemblies is supported by the building platforms through hangar rods and bolting arrangements so that no load is exerted on the test vehicle by the test hardware. Soft, highly compliant sealing hoses provide the only contact between the horn/duct systems and the test vehicle. The sealing hoses run longitudinally along the vehicle and separate the horn/duct walls from the vehicle surface. Acoustical isolation between adjacent horns and adjacent ducts is provided by the sealing hoses without interference with the vibration response of the surface of the test vehicle. During assembly of the horns and ducts around the vehicle, illumination checks are made with electrical lights for duct leaks which, when found, are eliminated by the application of rubber sealing compound. A hyperbolic-exponential design with an aspect ratio of 0.6 was used for the expansions of all horns, and a design cut-off frequency of 25 Hz was used throughout with the exception of the reverberant flare sections where 50 Hz had to be used because of space limitations (fig. 16).

The air modulators (fig. 17) are connected to the top of the initial horns with a quick-disconnect arrangement. Ancillary equipment items, including a cooling system

and a dc field supply, are located on adjacent platforms. The air modulators are linear-vane devices with electromagnetically driven cylindrical valves and were developed specifically for the SAL. The units are water cooled with a vacuum-assisted return system. The modulator valves are suspended on continuous rubber diaphragms and are driven inductively by variable electrical programing signals interacting with magnetic fields (ref. 7).

Control and Instrumentation

The control system equipment, located in a room adjacent to the acoustic tower, consists of 16 control and power channels, one for each of the 16 air modulators (fig. 18). Each channel includes a separate electrical white-noise generator and 1/3-octave band shaper for random programing, and a separate 3000-watt-power amplifier so that acoustic energy which is uncorrelated between ducts can be produced by the separate air modulators. The amplified programing signals are connected via cables to the air modulators in the tower. Through patching changes, one white-noise generator and shaper can be used to drive all amplifier and air-modulator channels to obtain an all-correlated acoustic condition between the ducts. Intermediate correlation combinations are also possible. Oscillators are available and the air modulators can be driven sinusoidally, or sinusoid programing can be mixed with random programing. While versatility of control is provided, a single master-gain control is used to increase and decrease the output levels of all air modulators simultaneously during a test run. Rapid attainment either of test levels or of shutdown was designed into the system to minimize undesired excitation and structural fatigue of the test vehicle. Other operational features include equipment malfunction alarms and automatic shutdown; emergency termination switches for the amplifier system and the air compressor; an arrangement allowing for selection of any control channel for monitoring by the test conductor; an environmental condition (temperature, humidity, and pressure) recording system; a flexible control and data instrumentation patching capability; plug-in modular components for quick replacement of malfunctioning units; intercom and television systems; and an analog data acquisition system consisting of signal-conditioning amplifiers and magnetic tape recorders. Presently, the data acquisition system can accommodate simultaneously 35 channels of horn/duct microphone measurements, 160 channels of test vehicle microphone and accelerometer measurements, and 50 channels of strain gage measurements. Multiple test runs with repatching can be used to obtain a larger number of response measurements on the test vehicle.

Each air modulator is calibrated using a plane wave tube (especially constructed for the purpose) before being installed in the SAL for a testing operation. All tests of airframe vehicles are preceded by a calibration test series using a boilerplate vehicle. During these calibration tests, the amplitudes and spectral shapes are adjusted sequentially in each duct at planned test levels. This procedure assures appropriate compensation for individual air-modulator/duct anomalies that may be present, and assures correct settings at high levels where acoustical nonlinearities occur. The controls for each channel are then documented and the test stack is torn down. The boilerplate vehicle is replaced with the actual spacecraft test article and the horn/duct systems reinstalled. A low-level test run for checking the test environment and for ranging of data acquisition equipment precedes high-level runs. For the high-level runs, the test conductor uses a single master-gain control to apply acoustic excitation

to the vehicle. Tape-recorded test data can be reduced with either analog or digital equipment at data reduction facilities located elsewhere at NASA MSC.

FACILITY PERFORMANCE

The major features of the facility performance for both the progressive wave duct and the reverberant modes of operation are reviewed in this section. In addition, some of the detailed performance characteristics of the coupling horns and ducts are examined, and the problems associated with coupling the progressive wave duct to the vehicle are discussed. Vibration responses, which are obtained with accelerometers at three locations on the SLA, are compared for both progressive wave duct and reverberant excitation. Vibration responses are presented which were obtained with accelerometers at eight locations on the SM, for both progressive wave duct and flight excitation.

Progressive Wave Performance

As described in previous sections, the progressive wave mode of operation allows variation of the overall SPL axially along the test article for all stations below the CSM shoulder. Furthermore, the progressive wave mode allows freedom in selecting the spectrum and level for each duct and the correlation parameters among various ducts. Therefore, for any individual duct, the spectrum throughout the duct has a definite relation to the spectrum at all other points along the duct. The relationship may be varied only by changing the axial variation of the duct cross-sectional area, the characteristics of the acoustical termination, or the axial impedance characteristics of the vehicle.

Air modulators were designed to meet the requirements of the SAL, and provide a maximum of 10 000 watts acoustical power output over a frequency range of 30 to 1000 Hz. The high-frequency performance of the facility is thus limited by the capability of the noise source above 1000 Hz, whereas the low-frequency performance is controlled by the horn cut-off characteristics and the terminating impedances. Within these frequency response constraints, a large variety of spectra can be generated, as indicated by the range of spectra measured in several experiments at the CSM shoulder, station X_a 1008 (fig. 19). Figure 20 shows that the overall level can be varied over at least 30 dB from 140 to 169.5 dB at the CSM shoulder station. Note that these particular spectra were chosen for specific experimental objectives and do not represent all possible spectra. For example, spectra which peak at either the low-frequency, middle-frequency, or high-frequency ends of the overall envelope indicated in the figure may be produced.

Figure 21 gives the spectra resulting at the Apollo shoulder for one setting of the electronic spectrum shaper and for various voltage amplitudes across the air modulator. Note that all spectra are essentially similar below 500 Hz. However, in the frequency range above 500 Hz, the rolloff for the high-level spectra is considerably less than for the lowest level spectra. This nonlinear property, termed macrosonic attenuation, results from the distortion of high-level acoustic energy in its propagation in

the initial horn. The distortion produces a triangular waveform which, when fully developed, will give a rolloff of approximately 3 dB per octave. For the data in figure 21, the highest level spectra is approaching the theoretical 3-dB per octave rolloff.

For some applications, the presence of distortion at high frequency is undesirable. However, the distortion is most useful for the majority of applications since it provides the only currently available method of extending the spectrum beyond the controllable limits of the acoustic noise source.

The variation of SPL along the axis of the vehicle is accomplished by varying the cross-sectional area of the ducts. The variation permits a change of area along the SM from the 90-sq-in. fixed cross section at the shoulder to as much as 450 sq in. at the base of the SM. The area along the SLA can vary from a minimum of 90 sq in. at the top of the SLA to a maximum of approximately 750 sq in. at the base. Part of the variation along the SLA comes from the increase in diameter of 13 feet at the top to 22 feet at the base, and the remainder comes from the ability to vary the radial dimension (or depth) of the duct from 4-1/2 to 15 inches.

Figure 22 illustrates the axial range of variation of SPL which has been found for the Apollo configuration. The ideal variation of SPL for both minimum and maximum duct spacings compares very closely with that measured in the high-frequency region. At low frequencies, however, the decrease of SPL along the vehicle is greater than that resulting from the area variation alone. The effect of frequency is best illustrated in figure 23, which gives the measured 1/3-octave band spectra in decibels relative to the shoulder spectra for four locations down the side of the test article. The high-frequency levels in figure 22 represent the average of the three 1/3-octave bands centered on 800 Hz (from fig. 23); the low-frequency levels were derived from the six 1/3-octave bands centered on 112 Hz.

Thus, figure 23 shows that the transition between the low- and high-frequency region occurs just above 250 Hz. As will be seen later, the maximum absorption of acoustic power by the vehicle structure occurs just below 250 Hz, with a considerable decrease in acoustic absorption at higher frequencies. Therefore, the additional decrease in SPL along the axis of the vehicle for the low-frequency region is attributed to the absorption of acoustic power by the vehicle.

The mechanism for this absorption can be seen from a simplified acoustic model of the duct/vehicle system as a duct with a continuous resistive absorber forming one side. Analysis of the model indicates that the attenuation in decibels along the duct due to absorption of acoustic power should vary directly with axial distance and inversely with radial duct dimension (or depth) for the Apollo structure. Therefore, if a lesser low-frequency SPL gradient along the vehicle were desired, the depth of the duct at the shoulder would need to be increased to obtain lower attenuation. Of course, the increase of area at the shoulder will have a side effect of reducing the maximum SPL in the duct at the shoulder. The simplified analysis also suggests that if the progressive wave duct mode of testing were utilized for vehicles of lower surface weight than that of Apollo (approximately 2 lb/sq ft), careful consideration would have to be given to the duct depth versus SPL gradient requirements.

The utilization of 16 ducts and their associated air modulators enables a controlled variation of the circumferential spatial correlation of the sound field along

the vehicle. As discussed in previous sections, this acoustic system, together with its electronic controls, can operate in any mode from "all ducts correlated" to "all ducts uncorrelated." The practical achievement of the "all ducts correlated" condition is yet to be demonstrated in the facility. Early experiments revealed that unity correlation was difficult to maintain from duct to duct over a wide frequency range, primarily because of variations among the acoustic noise sources. These variations among noise sources also made it difficult to obtain identical spectra and amplitudes among the ducts. The variation in SPL or in the 1/3-octave band sound pressure levels for all 16 ducts operating in the uncorrelated mode is shown in figure 24. As shown from the data envelopes, when the overall sound pressure levels are controlled to within ±1-1/2 dB, the sound pressure levels in 1/3-octave bands remain within ±2 to 3 dB over a substantial portion of the frequency range. However, deviations up to 4 dB are noted in the high-frequency end of the spectra. The increase in deviation in high frequency for the spectra is associated with the fact that the levels in this frequency range are generated both by controlled modulation and nonlinear distortion of noise from lower frequency modulation. In any event, the overall variation illustrated in figure 24 is considered quite acceptable for practical test purposes.

A great number of interesting experimental results have been derived from the facility. Many of these experiments are directed toward obtaining better understanding of detailed factors which affect the overall performance of the facility. Although space does not permit discussion of all investigations here, two of the detailed factors have general application to progressive wave duct excitation of aerospace vehicles and will be discussed briefly in the following paragraphs.

Horn Performance

In the design of a high-intensity acoustic facility, horns are employed to give a smooth transition from the very small area of the air-modulator throat to a large area at the entrance to a test section. Ideally, the horns should be perfectly terminated in impedances which match the characteristic impedance of air (or ρc) and act as perfect couplers for the energy over the entire frequency range. However, in any finite-length horn/duct system, the termination is always less than perfect and will cause reflected waves. The reflections result in the buildup of standing waves, which may be found experimentally by probing the sound field along the axis of the horn. A typical result of such a probe is given in figure 25 for the initial horn and for three discrete frequencies.

At 400 Hz, a variation of SPL along the axis departs from the ideal horn area expansion by less than 1 dB. However, at 100 Hz and lower frequencies, a greater difference is found between the ideal and the real horn. The difference can be quantified in terms of the standing wave ratio, which is the peak-to-peak difference in decibels of the departure of the pressure amplitude from the mean. This behavior can also be related to the effective absorption coefficient of the termination to the horn (and is a measure of the quality of the termination).

Both the standing wave ratio and the effective absorption coefficient for the initial horn, reverse horn, and reverberant flare horn are given in figures 26(a), 26(b), and 26(c), respectively. The effective absorption for the initial horn approaches 100 percent for frequencies above 150 Hz. However, below 100 Hz, the absorption varies between 70 and 90 percent, depending on frequency and type of termination. Although

the absorption for most acoustical purposes is generally of primary interest, the standing wave ratio is perhaps more meaningful from the point of view of assessing facility performance, since it gives twice the maximum deviation from the mean SPL in terms of decibels. Also, as seen in figure 26, the standing wave ratio is a more sensitive indicator than the absorption coefficient in detecting minor departures from the ideal.

Duct Seals

The sealing of the individual ducts to the vehicle to prevent leakage of sound into adjacent ducts is necessary to maintain independent noise fields and for the adequate acoustic termination of each noise source. A leak along the duct acts as a distributed inductive shunt and causes a significant degradation of the low-frequency performance of the entire system, in addition to providing added attenuation along the duct. The potential seriousness of the situation is illustrated in figure 27, which gives results from a one-third scale model of a typical duct section studied during the design of the facility. Spectra are given for three stations located in the parallel section of the duct, varying between 2 and 80 inches from the interface between the horn and duct. The data for the 2-inch location in figure 27 demonstrate that the overall frequency response of the horn/duct configuration rolled off below 100 Hz. However, with a tightly sealed configuration, the low-frequency performance is significantly improved with the low-frequency cut-off occurring at approximately 30 Hz. Furthermore, the results for locations farther down the duct show that considerable attenuation is occasioned by the leak.

These two effects of improper sealing make it essential to seal the vehicle to the duct acoustically. However, the sealing requirement conflicts somewhat with the requirement that the presence of the duct shall not inhibit the vibration response of the vehicle. This potential problem area was recognized early in the design concept study and resulted in experimental studies of various types of sealing devices to meet both criteria. The final result for the ducts along the Apollo vehicle is a 1-inch-diameter rubber hose of low durometer, supplemented with plastic sealants over local contour variations about the vehicle mold lines.

The noise reduction between adjacent ducts (fig. 28) is approximately 15 to 20 dB over both the CM and the SM. However, the noise reduction between these same ducts, when measured at the base of the SLA, is only 5 to 10 dB for frequencies below approximately 300 Hz and increases to approximately 20 dB above that frequency. This lower noise reduction at the base of the SLA is suspected to result from the reradiation of energy by the vehicle into adjacent ducts. This would also explain the increase of the noise reduction to the 20-dB level at frequencies above the principal response frequencies of the vehicle, as discussed previously and exhibited in the axial attenuation of figure 22.

The seal design, which gives a reasonable noise reduction, simultaneously enables achievement of designed low-frequency response performance characteristics.

To test the possible interference of the sealed ducts with the vibration response of the vehicle, experiments were conducted in which the vehicle was mechanically excited, both with and without the acoustic duct system. A typical vibration response,

measured in 1/3-octave bands, for a boilerplate CM is given in figure 29 for both cases. For convenience, the vibration response is expressed in decibels relative to 10^{-6} g. Little variation was experienced throughout the spectrum. Figure 30 gives a summary of the differences in response measured in the SLA at six accelerometer locations for mechanical excitation, both with and without the duct system coupled to the vehicle. Again, the variation appears to be within the statistical accuracy of the data. These and other experiments demonstrated that the seals currently in use are more than adequate for the Apollo vehicle. However, if vehicles of significantly lower surface weight were to be tested in a similar configuration, the adequacy of the seals would need to be demonstrated again.

Reverberant Performance

The second basic mode of operation provided in the SAL is the semi-reverberant mode discussed in a previous section. Although the principal experimentation to date has been with the progressive wave mode, the measurements with the reverberant mode indicate that it will also furnish a practical tool for certain Apollo test applications.

The acoustical absorption provided inside the SAL is given in figure 31. The absorption below approximately 1200 to 1600 Hz averages a little over 4000 sq ft, resulting in an absorption coefficient of approximately 0.12, based on a wall surface area. The absorption coefficient is approximately eight times higher than would be expected in a standard hard-walled reverberation chamber. However, it is not the result of the classical acoustic absorption expected from soft resistive absorptive materials; rather it is the result of the vehicle, of the steel gratings provided at every platform level, and of the various steel piping and other systems provided in the tower for general facility operation. The increase in absorption illustrated in frequencies above 1600 Hz is the result of natural air absorption in the room and is expected to become asymptotically proportional to the square of frequency.

Figure 32 gives the range of sound pressure levels measured along the SLA immediately adjacent to the skin and in the general chamber volume. The levels are the result of a reasonably flat input spectrum at almost full acoustic power. Note that the levels adjacent to the SLA are within 1 or 2 dB of those predicted for the launch case. Therefore, this configuration has utility for some test purposes utilizing the SLA.

The difference between the sound pressure levels in the general chamber volume and those adjacent to the actual structure, as illustrated in figure 32, is important to note. Although the usual practice for equipment testing is to specify and measure the average level in the general volume of a reverberant chamber, the levels which are most important for full vehicle testing are those adjacent to the skin. Thus, in designing a vehicle test, differences between the chamber reverberant level and the pressure on the skin of the order of those shown in figure 32 must be considered in specifying and measuring the test spectrum.

The relative spectra between the Apollo shoulder station and the four longitudinal stations along the test article are given in figure 33. These data, which are measured at the same stations utilized in figure 23, show the type of variation of axial sound pressures which might be expected from a combination of a close-coupled

horn/vehicle configuration in a reverberant chamber. Naturally, the absolute magnitude of the difference between the close-coupled region and the throat of the horn in the reverberant chamber is dependent on both the coupling area and the absorption of the chamber.

Vibration Response

The ultimate intent of the acoustic facility is to produce a vibration field within the vehicle which is similar to that actually encountered in its mission performance. The transfer function, which relates the average vibration within the vehicle to the surface acoustic pressures, is known to be a function of the type of external pressure of the fluctuating field. Figure 34 gives the transfer function for three accelerometers located on the SLA for both the progressive wave duct and reverberant field excitations. The data show that the shapes of the transfer functions are almost identical and the absolute magnitudes are similar, although the reverberant sound field appears to produce a response averaging approximately 3 dB higher than that produced by progressive wave duct excitation.

Note that the frequency response characteristics and the magnitude of the responses which govern the transfer functions are a function of the SLA structure, size, stiffness, mass, and damping, as well as the characteristics of the room and the method of excitation, and therefore cannot be applied to other vehicles without suitable correction.

Figure 35 gives the space average fluctuating pressure spectra measured on the surface of the SM during Apollo flights. In an attempt to match the SM vibration response in SAL, acoustic spectra (fig. 35) were applied to a prototype airframe (honeycomb structural shell) SM with the progressive wave duct configuration. Figure 36 presents the resulting two vibration response spectra for flight and laboratory cases. Each curve represents an average of eight accelerometers located on the SM outer shell with the locations in the laboratory test closely duplicating those in flight.

Further indications of good response simulations attainable in SAL are presented in another paper (ref. 6) discussing a specific test program in the facility.

CONCLUDING REMARKS

Simulation of vehicle vibration response to the acoustic waves propagating forward from the first-stage booster engine at lift-off is reasonably straightforward through application of progressive acoustic waves in the Spacecraft Acoustic Laboratory. However, simulation of vehicle vibration response to aerodynamically induced fluctuating pressures, through the transonic and maximum dynamic-pressure flight regimes (by using acoustic progressive waves in the laboratory), required adjustments to the correlation, amplitude, and spectral shapes of the laboratory composite wave energy. The laboratory acoustic environment applied to the vehicle is not necessarily a duplication, acoustically, of the flight fluctuating pressure environment when attempting to achieve duplicate vehicle vibration response in the laboratory. Until adjustment criteria can be developed for the wide range of fluctuating pressure

environments and the vehicle structural characteristics which are possible, testing will probably follow a two-step procedure. The first step will be to program the laboratory environment to match the measured or predicted service environment in accordance with the amplitude and spectral shape. Comparison of vehicle vibration responses obtained from the first step with service vibration responses will then lead to the second step of adjusting the laboratory environment conditions, including phase correlation coefficients, if possible, to achieve a duplication in the laboratory of the service vibration responses.

Checkout and development tests have proved the practicality and workability of the fluctuating pressure simulation approach embodied in the Spacecraft Acoustic Laboratory for full-scale ground testing of large vehicles. Examination of acoustic performance data has shown that the design requirements for the Spacecraft Acoustic Laboratory have been met or exceeded. Vehicle vibration responses, which closely duplicate responses measured in flight, have been obtained in the Spacecraft Acoustic Laboratory for the Apollo spacecraft.

The Spacecraft Acoustic Laboratory has been and currently is supporting the Apollo Program with evaluations of structurally complete prototype spacecraft. Further use of this unique facility in support of the Apollo Applications Program is scheduled, and application of this simulation technique to future programs (such as the Manned Orbital Laboratory and the Mars Mission), which will have vehicles with new shapes and sizes, is possible with merely a modification of a portion of the acoustic test hardware.

Manned Spacecraft Center
National Aeronautics and Space Administration
Houston, Texas, February 29, 1968
914-50-20-15-72

TABLE I. - CONTROL OF FLUCTUATING PRESSURE PARAMETERS IN THE SAL

[Neglecting protuberances and yaw]

Independent variable	Case	Function		
		Amplitude	Spectrum	Spatial correlation
Axial location	Flight	Depends on vehicle geometry and Mach number	Depends on vehicle geometry and Mach number	Depends on vehicle geometry and Mach number
	SAL	Determined by cross-sectional area of horns and ducts and by air-modulator output	Determined by finite length effects and absorption of power by vehicle and ducts and by air-modulator output	Cannot be varied
Time	Flight	Variable	Variable	Variable
	SAL	Stepwise approximation or possibly continuous variation	Stepwise approximation or possibly continuous variation	Stepwise approximation or possibly continuous variation
Axial separation	Flight	--	--	Variable
	SAL	--	--	Either cos ky in progressive wave mode or sin ky/ky in reverberant mode
Circumferential separation	Flight	--	--	Variable
	SAL	--	--	Variable to within one-sixteenth of circumference in progressive wave mode; approximately sin ky/ky in reverberant mode

NASA-S-68-1032

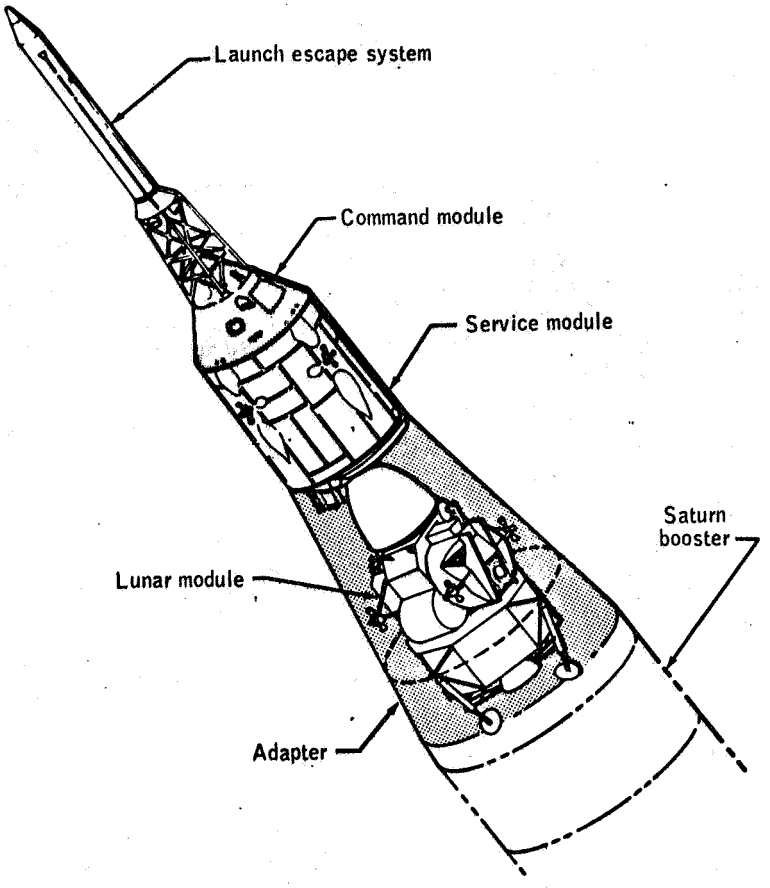

Figure 1. - Apollo spacecraft vehicle in launch and boost configuration.

NASA-S-68-1033

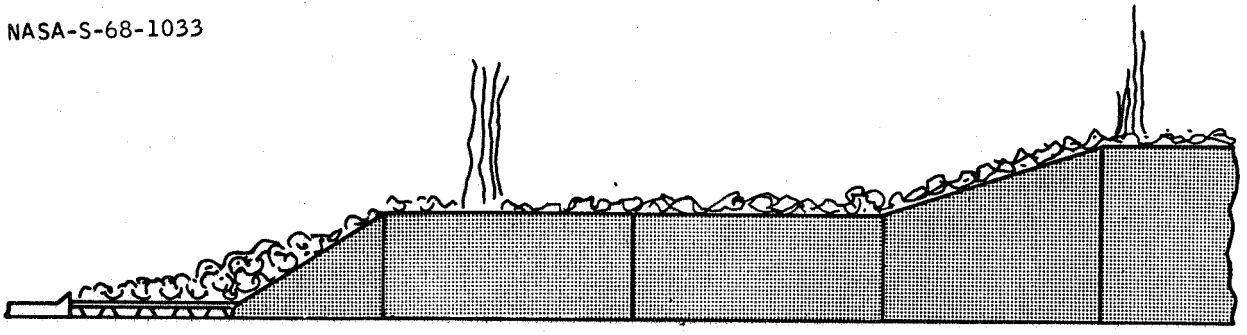

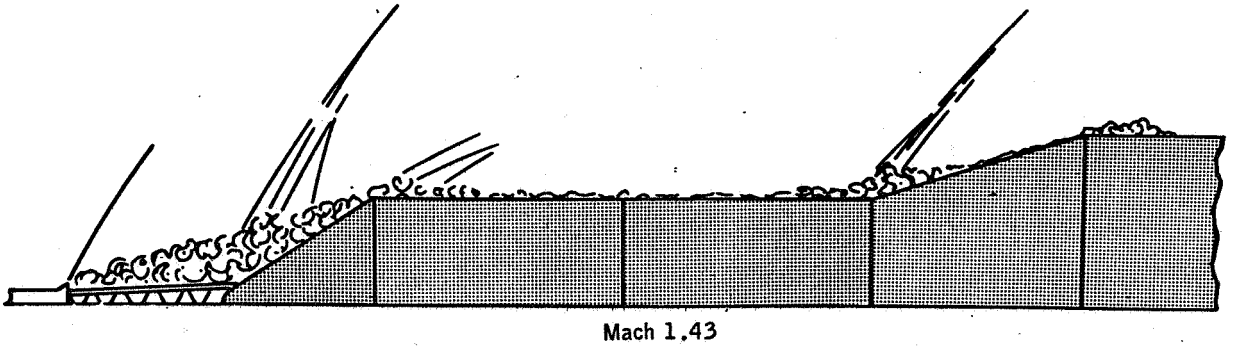

Figure 2. - Sketches of two flow regimes over the Apollo vehicle from Marshall Space Flight Center wind-tunnel tests (original SLA configuration).

NASA-S-68-1034

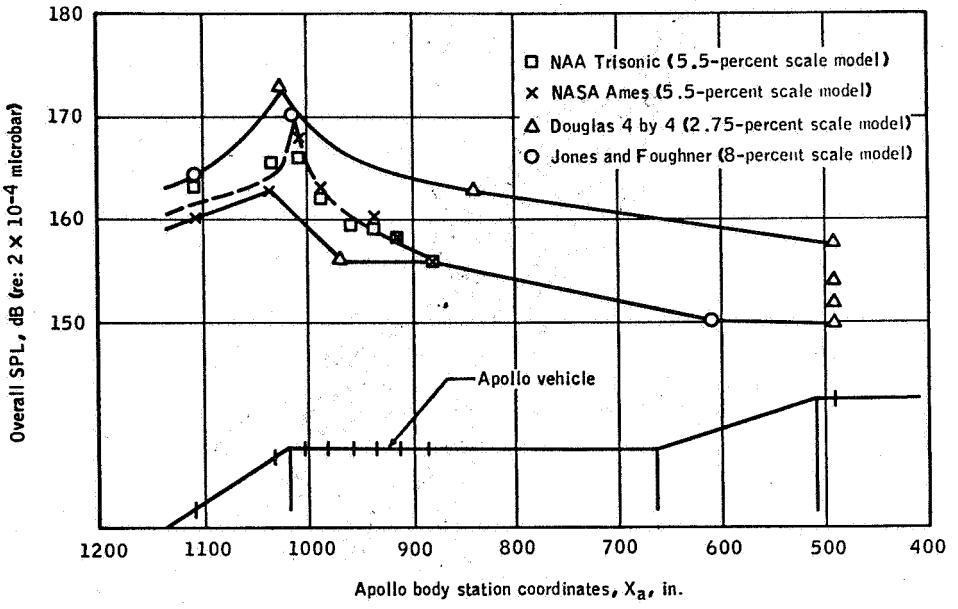

Figure 3. - Comparison of maximum overall aerodynamic pressure fluctuations found in previous studies of typical configurations corrected to flight dynamic pressure (original SLA configuration).

NASA-S-68-1035

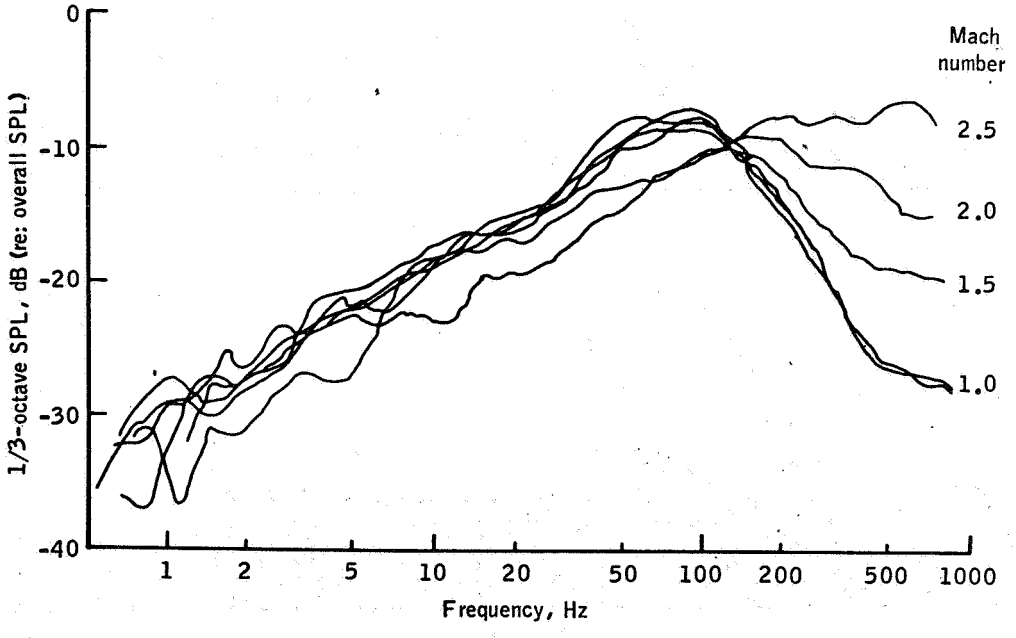

Figure 4. - Typical relative pressure spectra downstream of shoulder at various Mach numbers.

NASA-S-68-1036

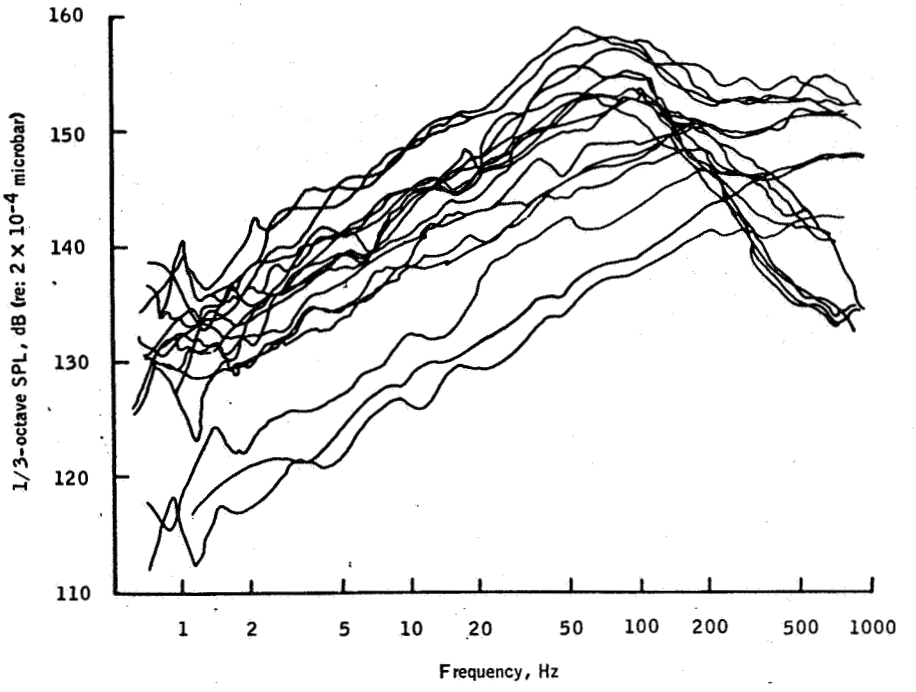

Figure 5. - Typical spectra of pressure fluctuations in 1/3 octaves for several positions and several Mach numbers.

NASA-S-68-1037

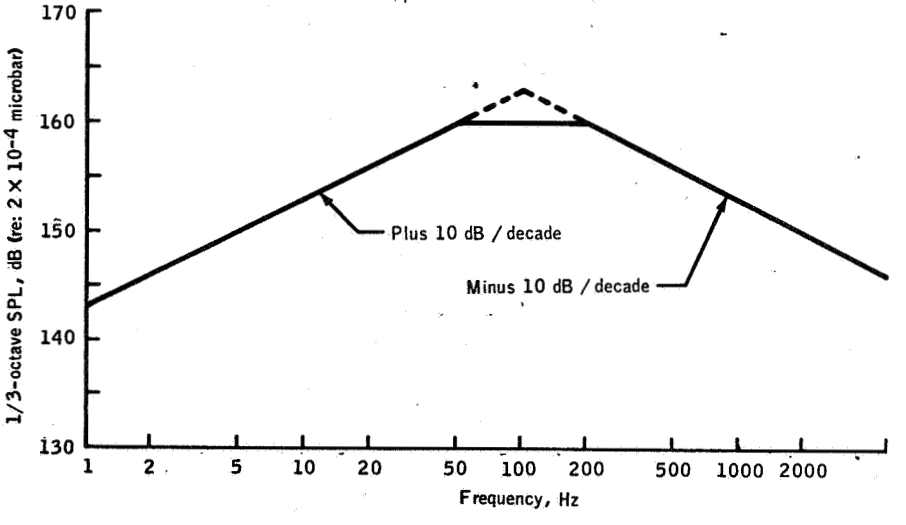

Figure 6. - Design curve for random noise spectrum at shoulder of Apollo vehicle with an overall level objective of 171 dB.

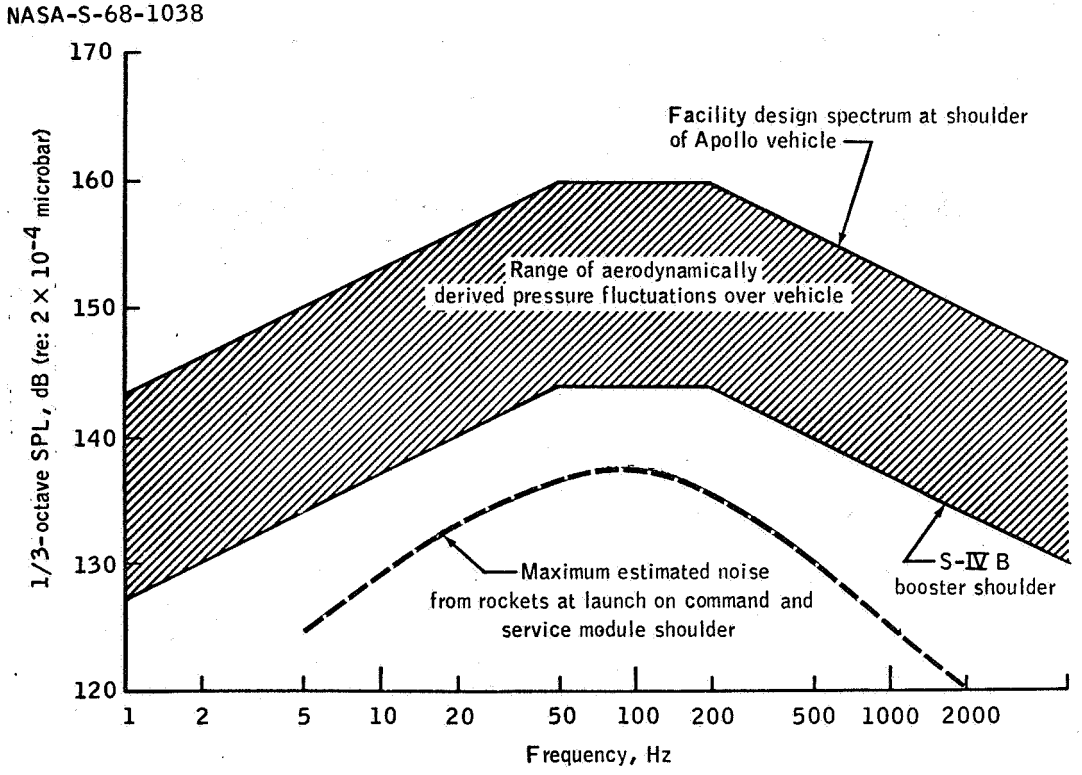

Figure 7. - Comparison of flight dynamic pressure fluctuations with facility design spectrum for Apollo vehicle.

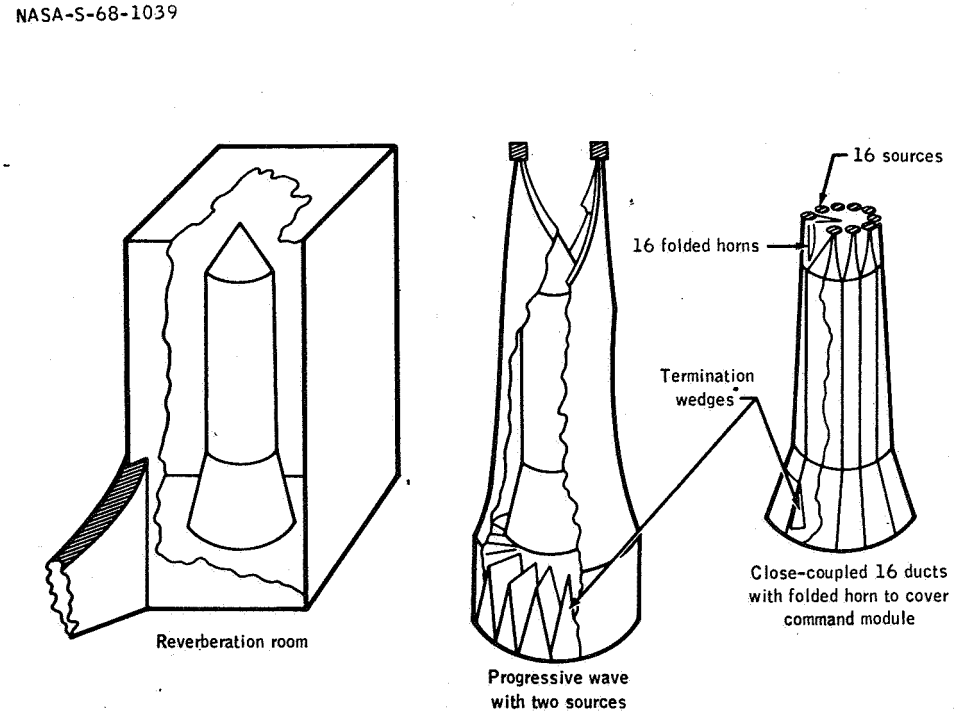

Figure 8. - Three facility concepts for SAL.

NASA-S-68-1040

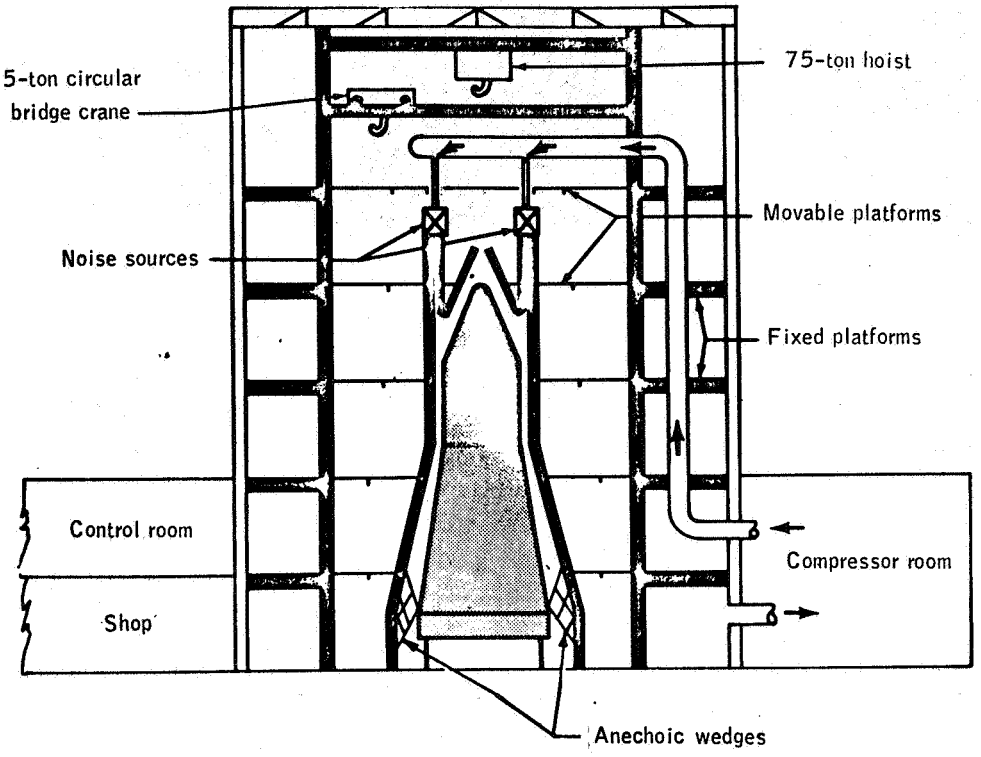

Figure 9. - Spacecraft Acoustic Laboratory.

NASA-S-68-1041

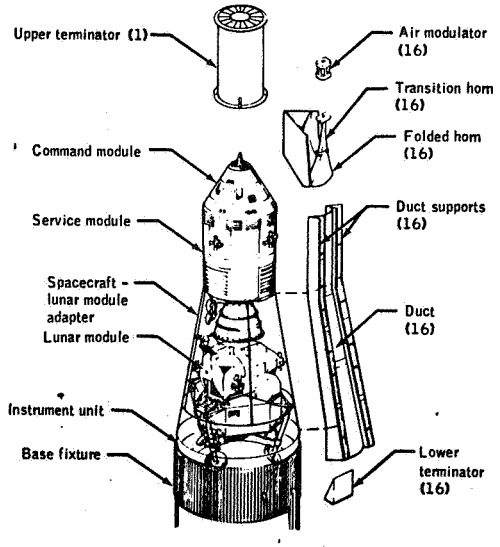

Figure 10. - Arrangement of test article and horn/duct system.

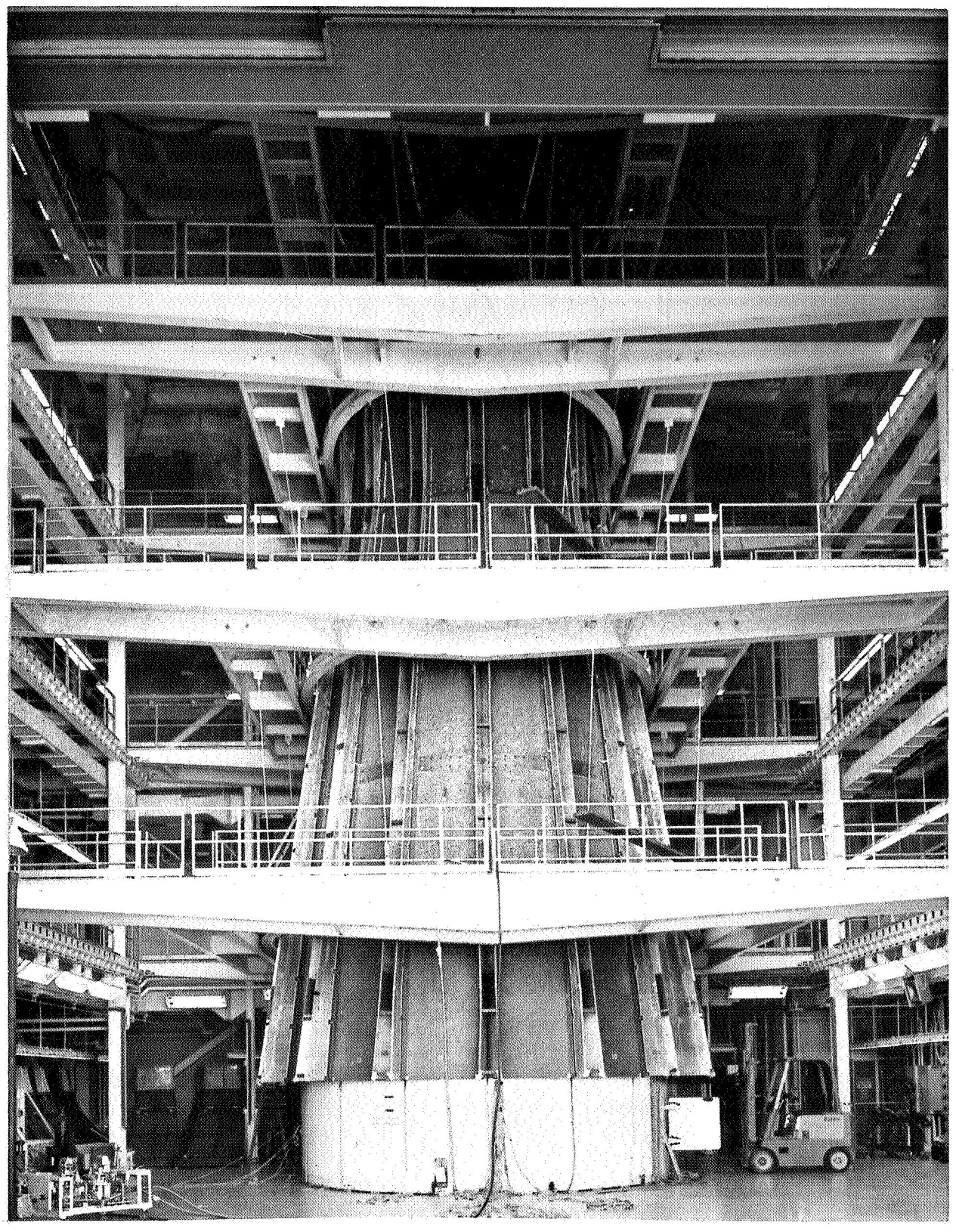

Figure 11. - Apollo vehicle in SAL after installation of duct system.

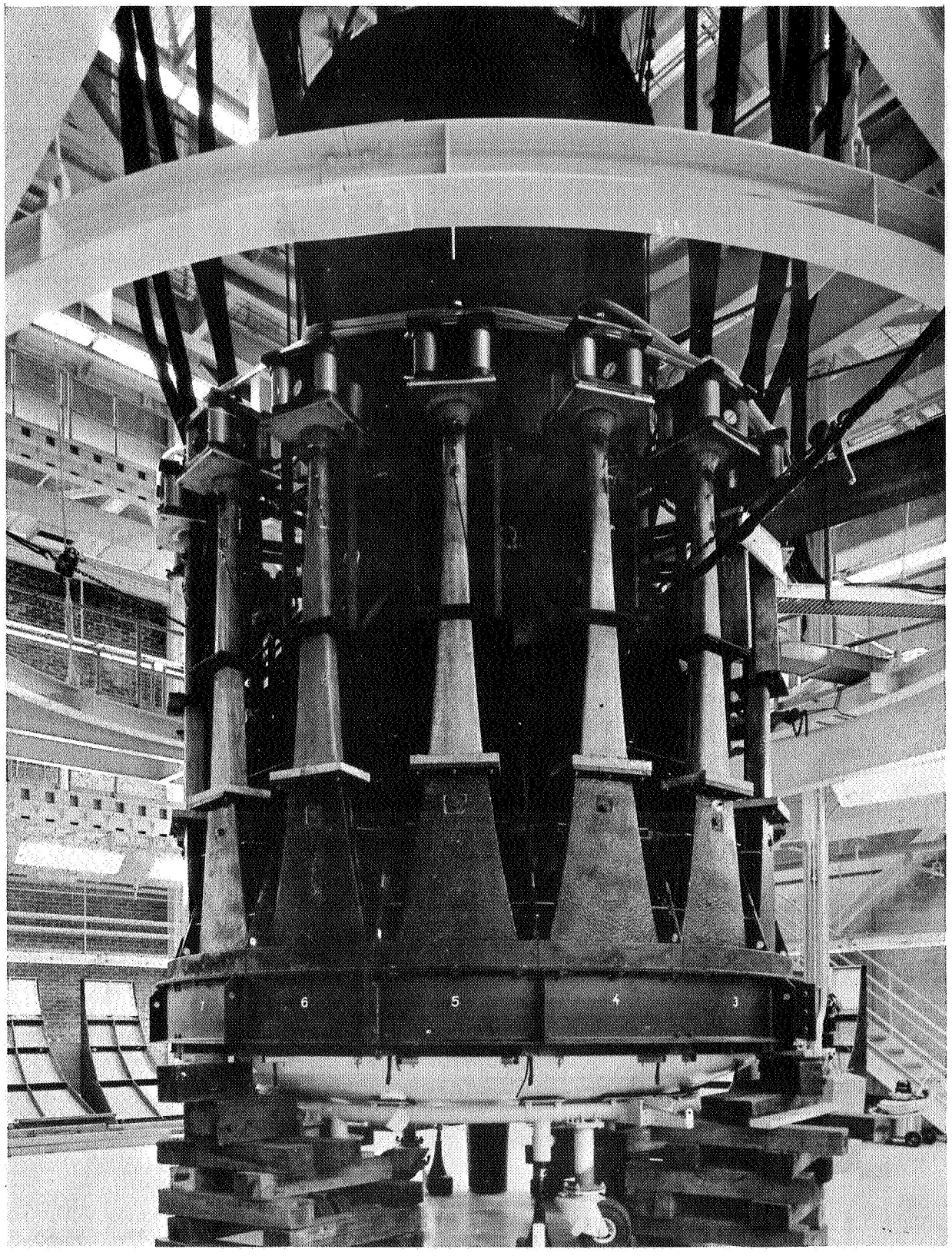

Figure 12. - SAL horn assembly with air modulators installed.

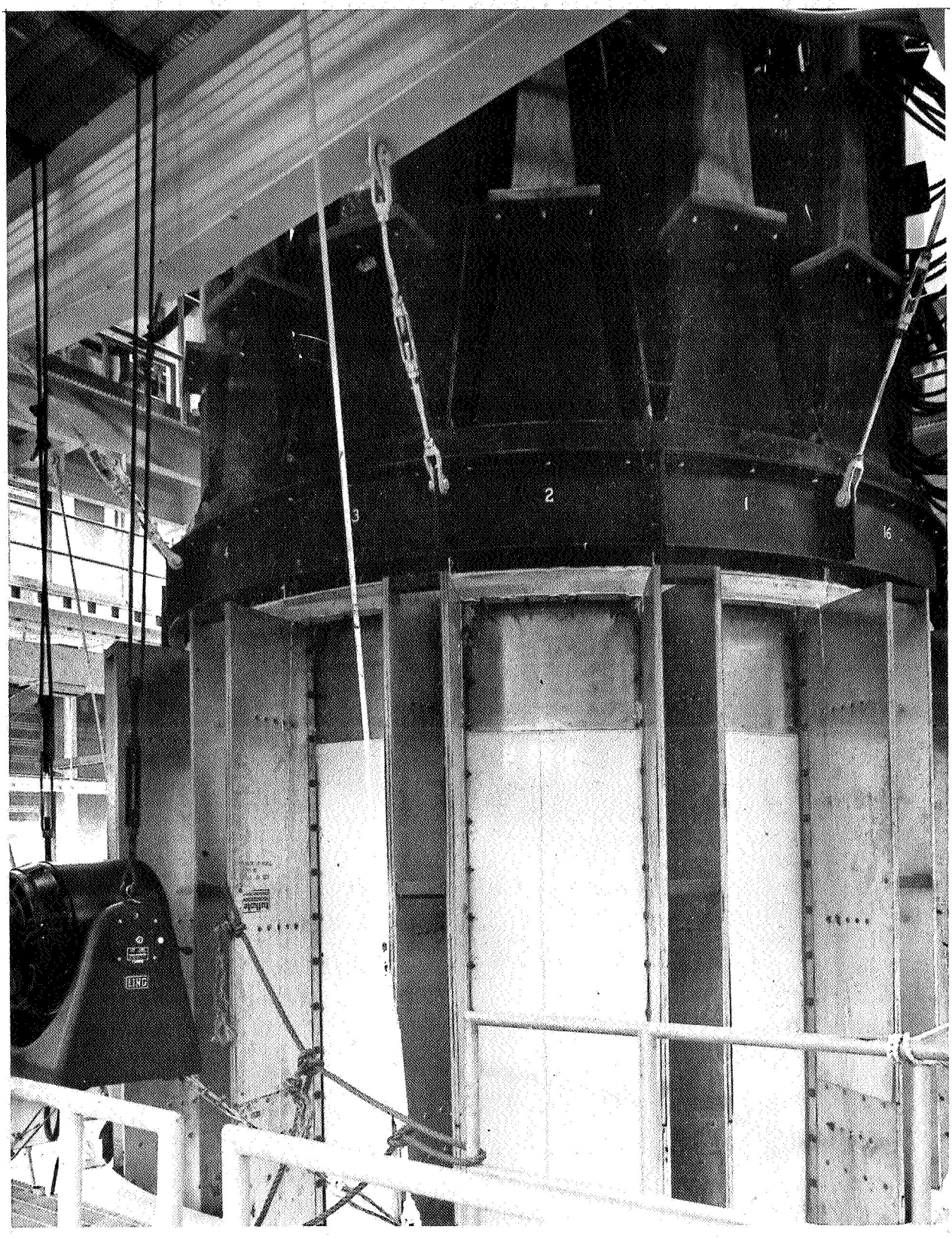

Figure 13. - Ducts removed showing contact of V-shaped duct supports with outer shell of SM vehicle.

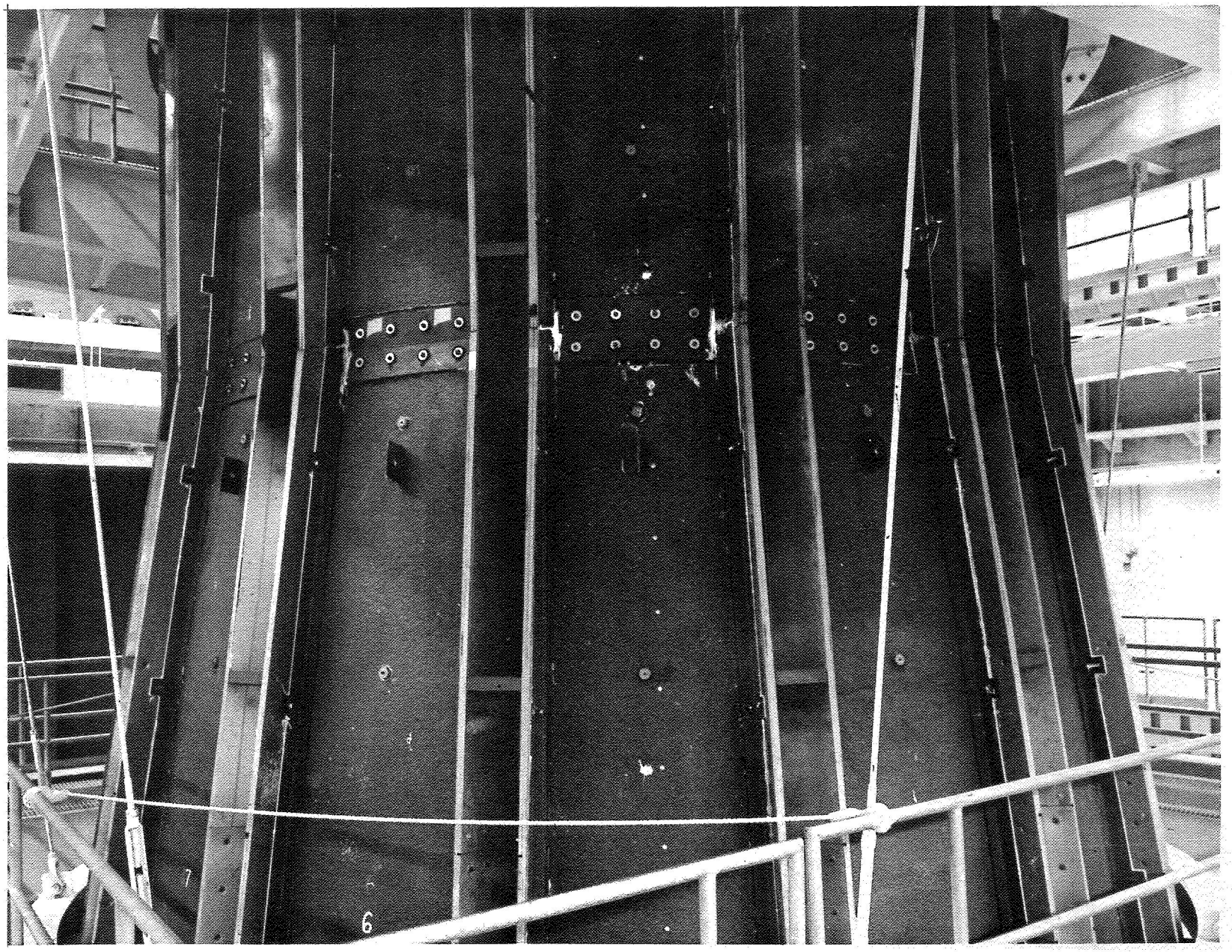

Figure 14. - Interface of SAL ducts covering SM with ducts covering SLA.

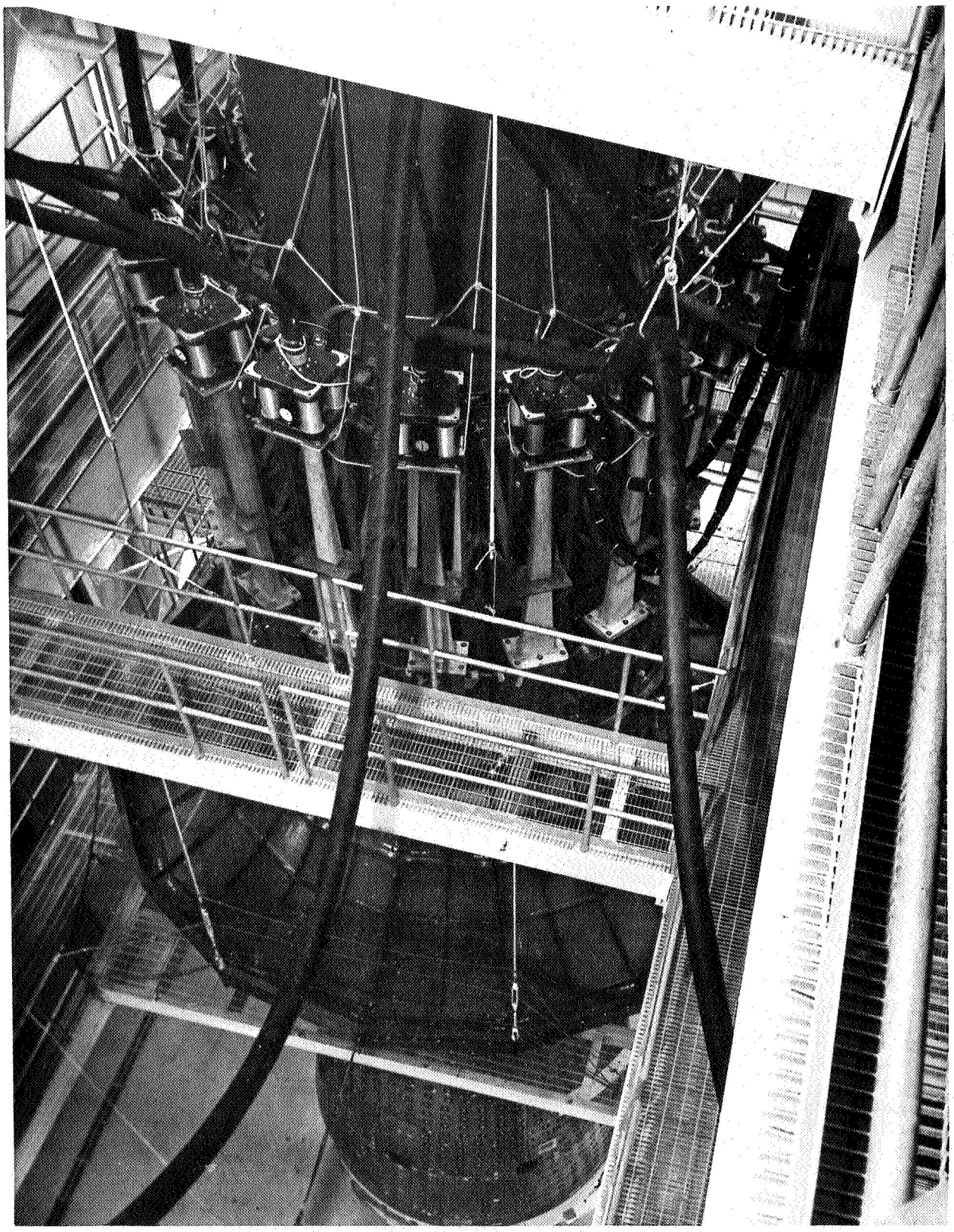

Figure 15. - SAL reverberant flare system installed around Apollo vehicle.

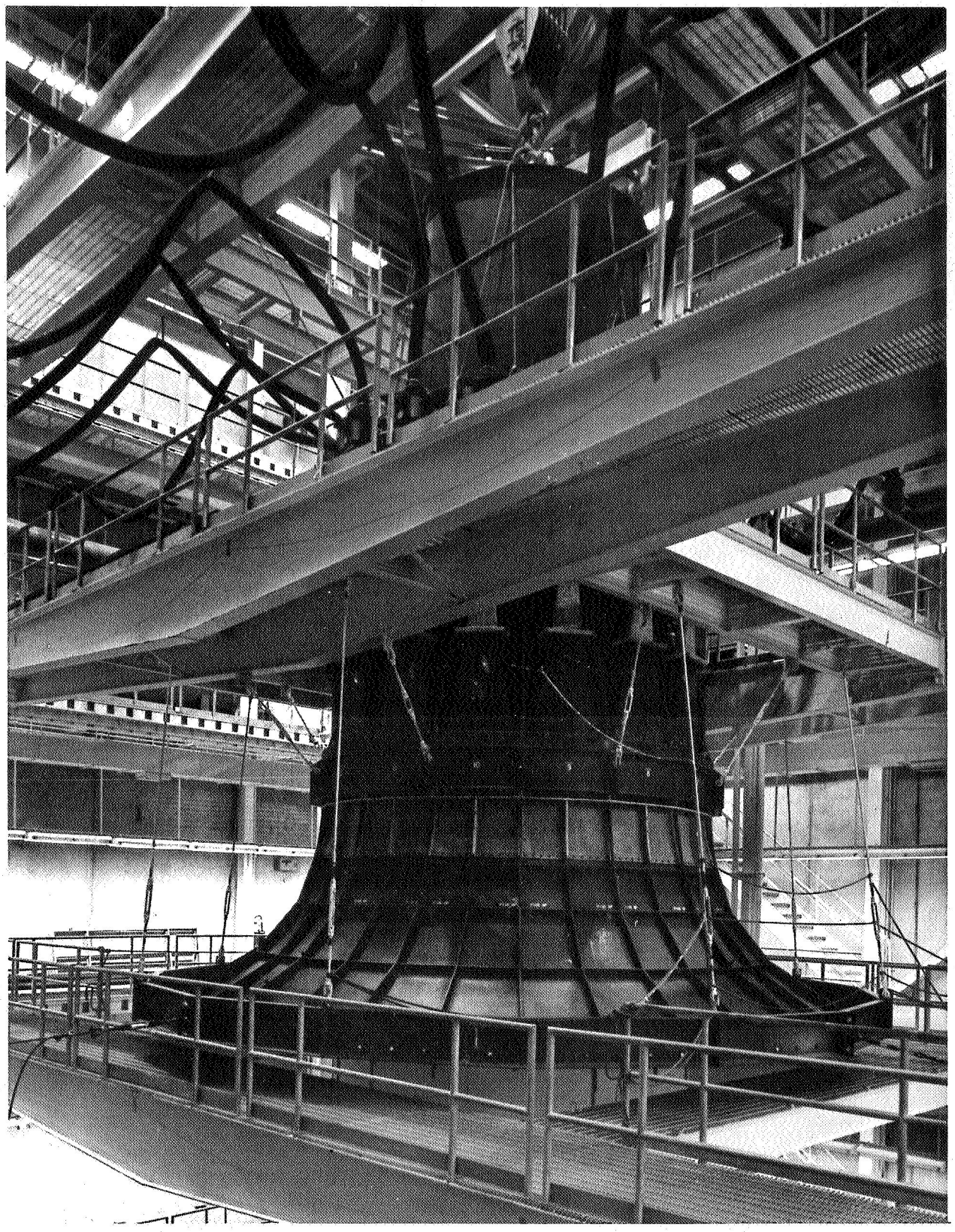

Figure 16. - SAL reverberant flare system.

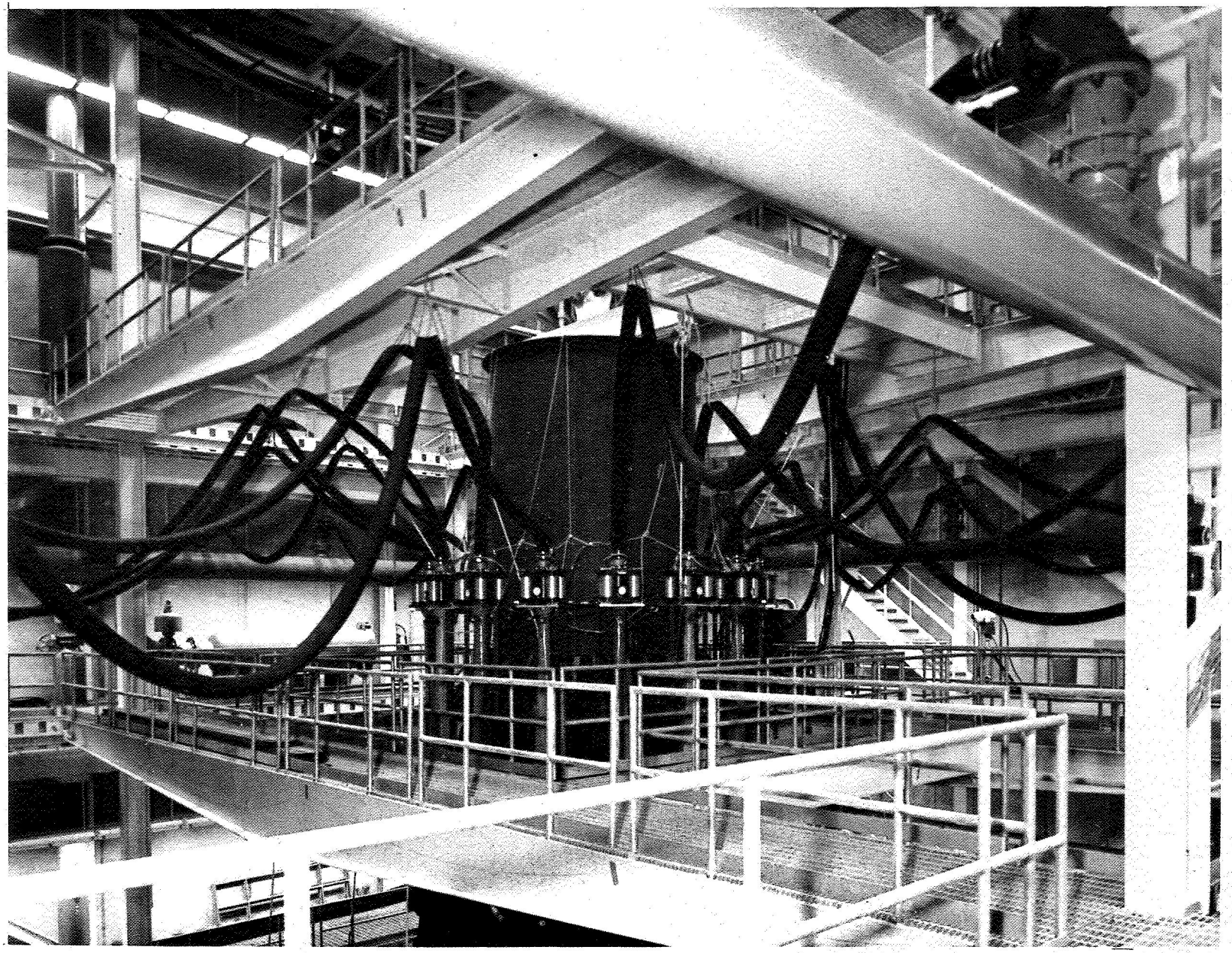

Figure 17. - Access to the horn assembly and air modulators of the SAL via movable platforms.

NASA-S-68-1049

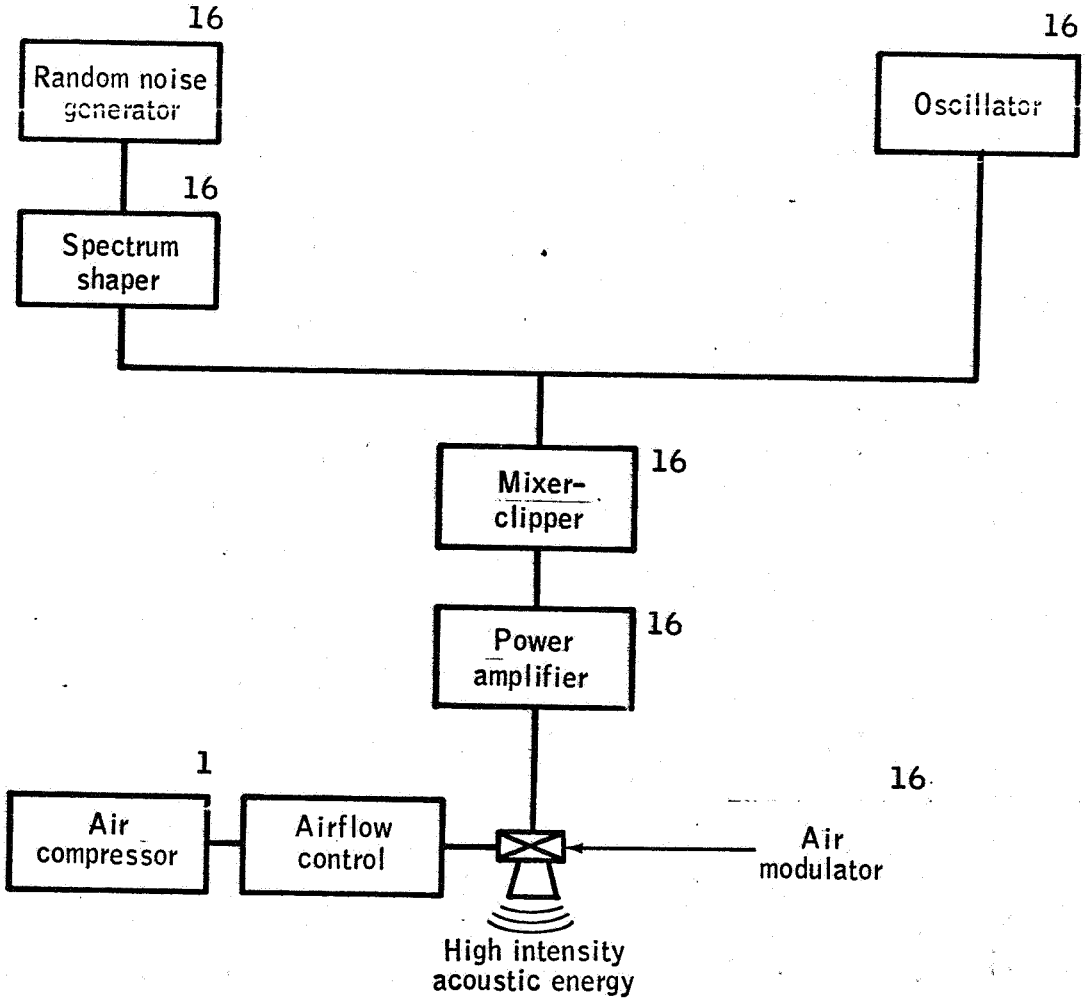

Figure 18. - SAL control system.

NASA-S-68-1050

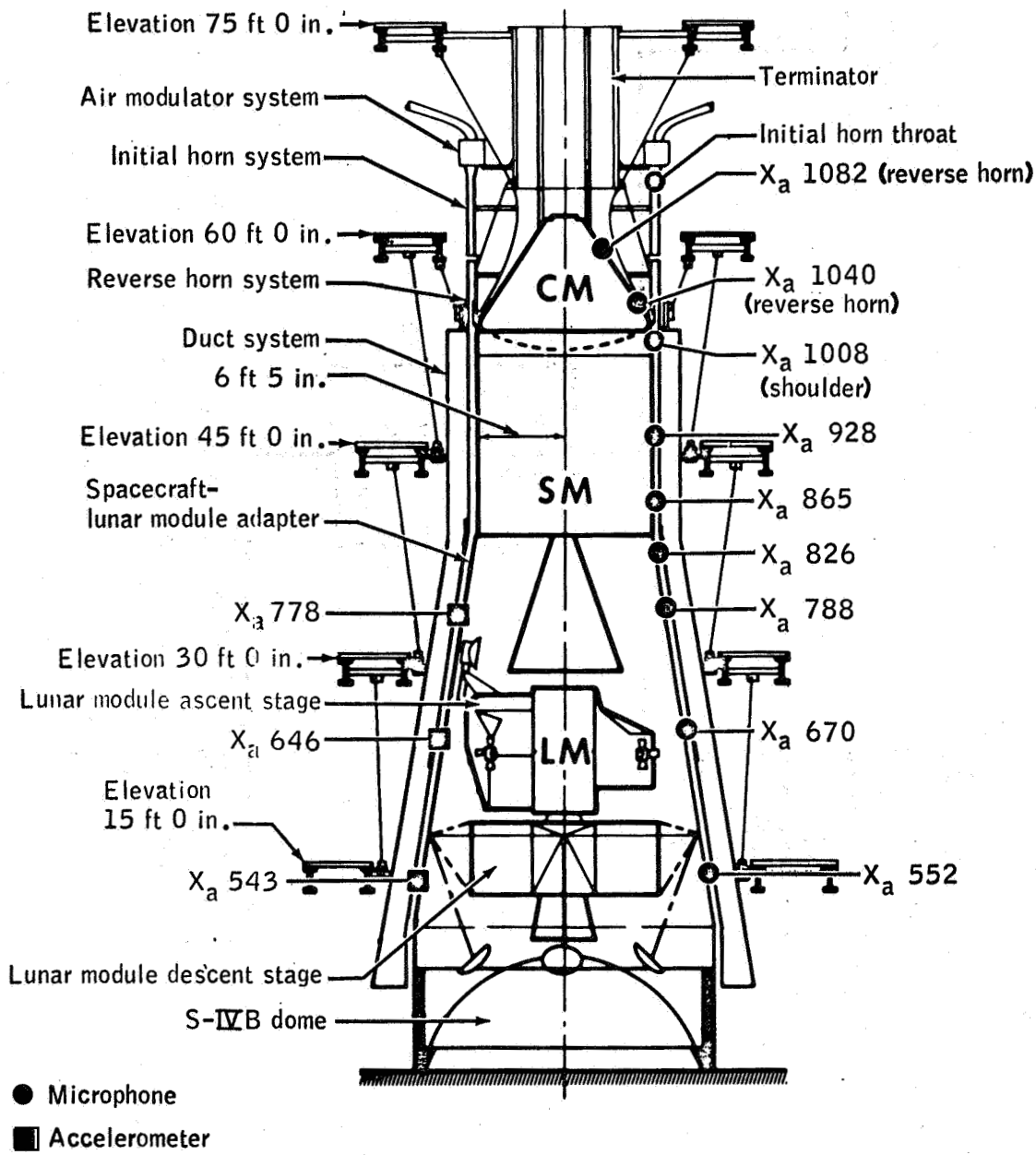

Figure 19. - Measurement locations for Apollo tests in the SAL.

NASA-S-68-1051

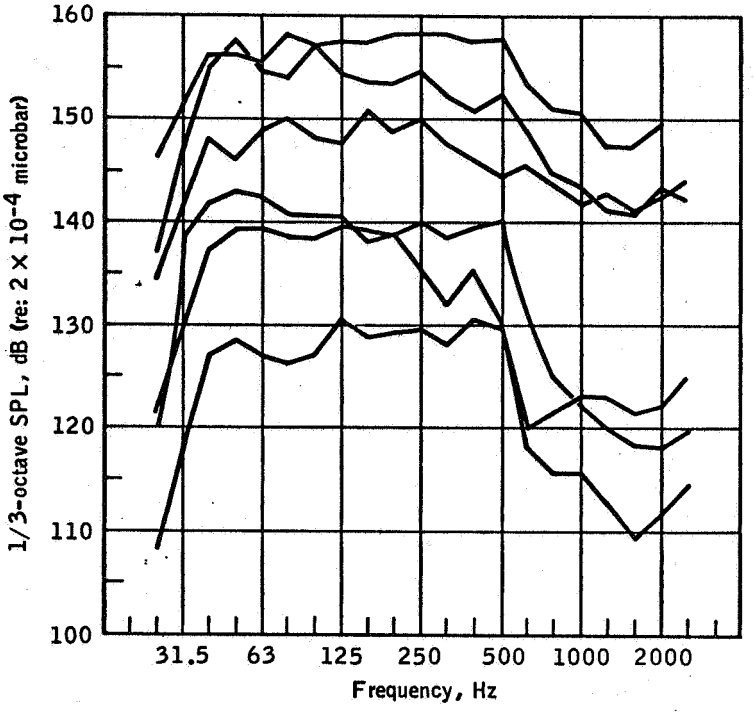

Figure 20. - Typical spectra in SAL at Apollo shoulder.

NASA-S-68-1052

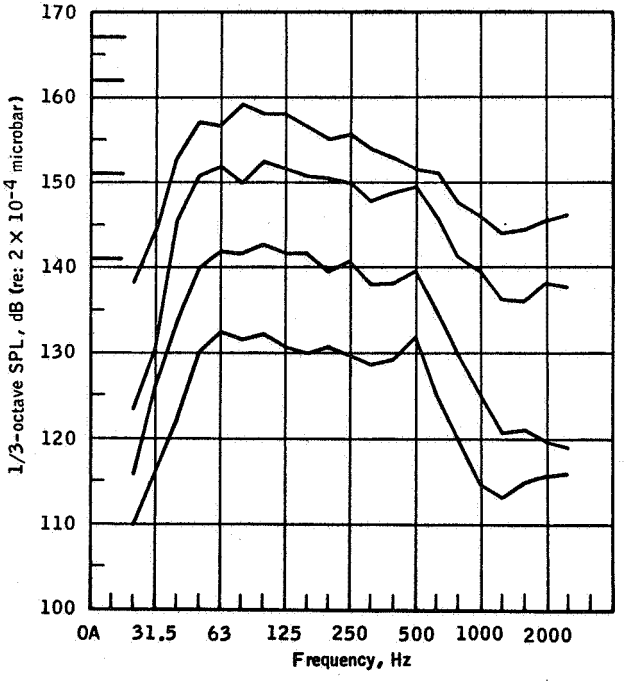

Figure 21. - Spectra obtained at Apollo shoulder in SAL by varying overall power input to noise makers.

NASA-S-68-1053

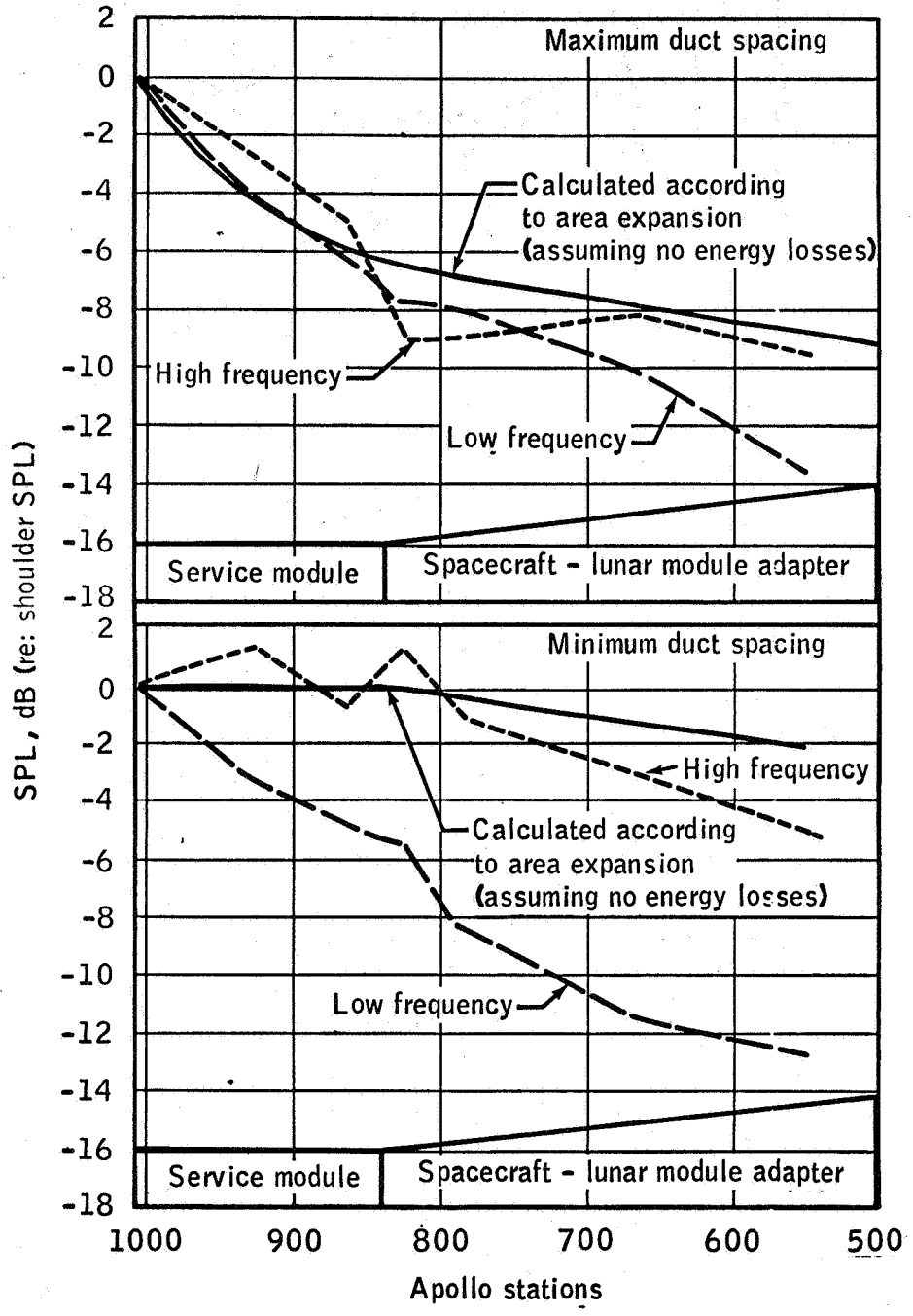

Figure 22. - Axial variation in SPL for maximum and minimum duct spacing.

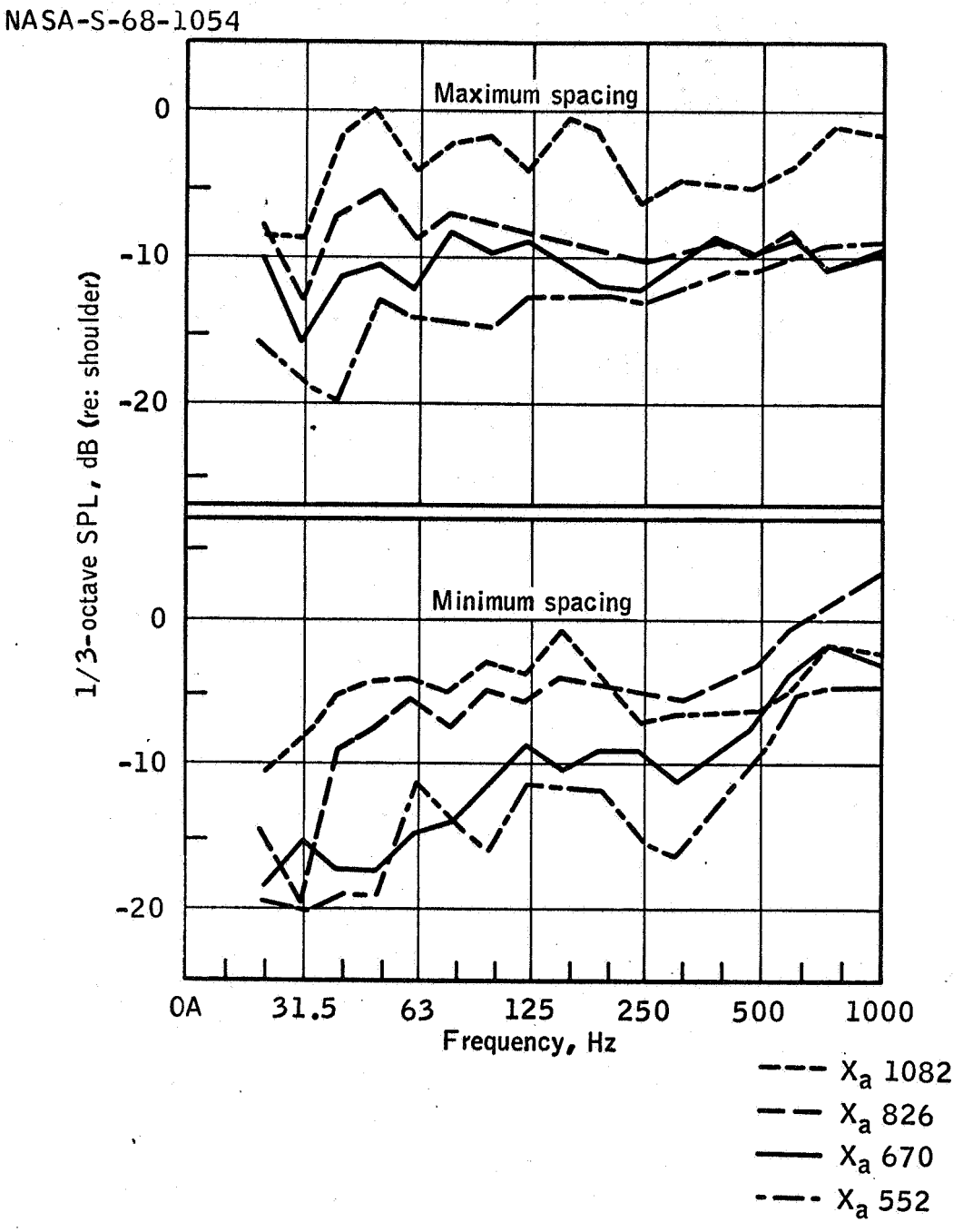

Figure 23. - Spectra in ducts for two duct spacings from Apollo.

NASA-S-68-1055

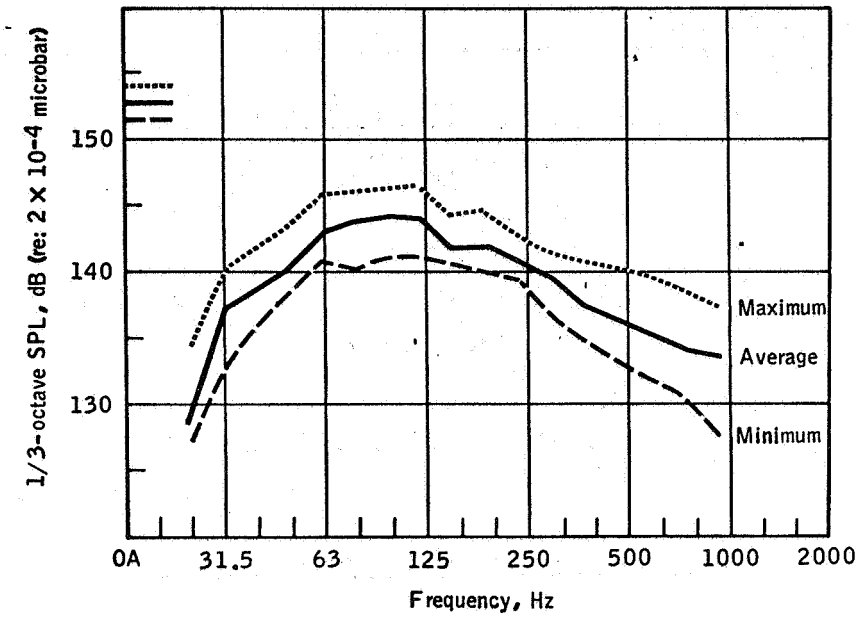

Figure 24. - Typical envelope of SPL variation in SAL for 16-duct operation.

NASA-S-68-1056

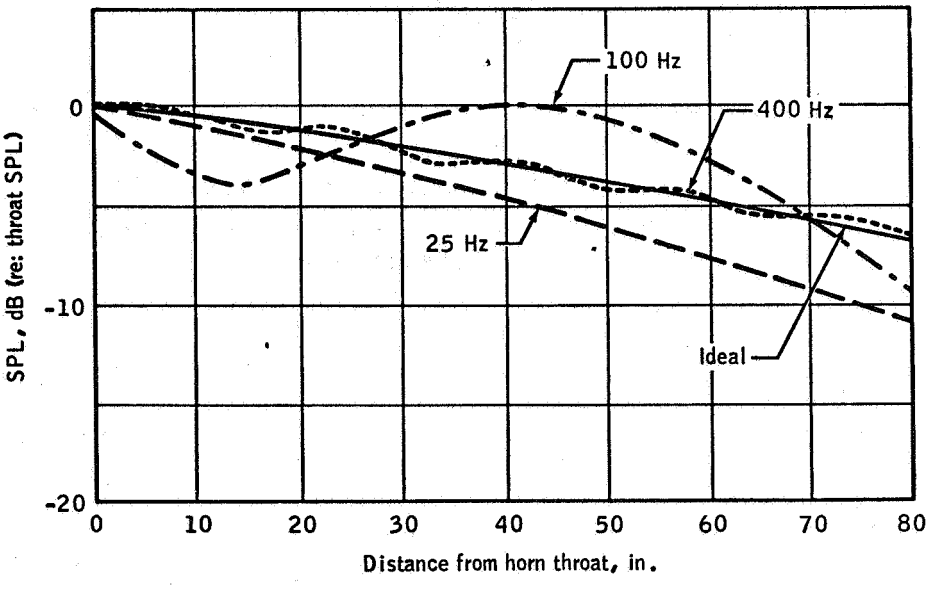

Figure 25. - Axial variation in SPL of initial horn for single frequency excitation.

NASA-S-68-1042

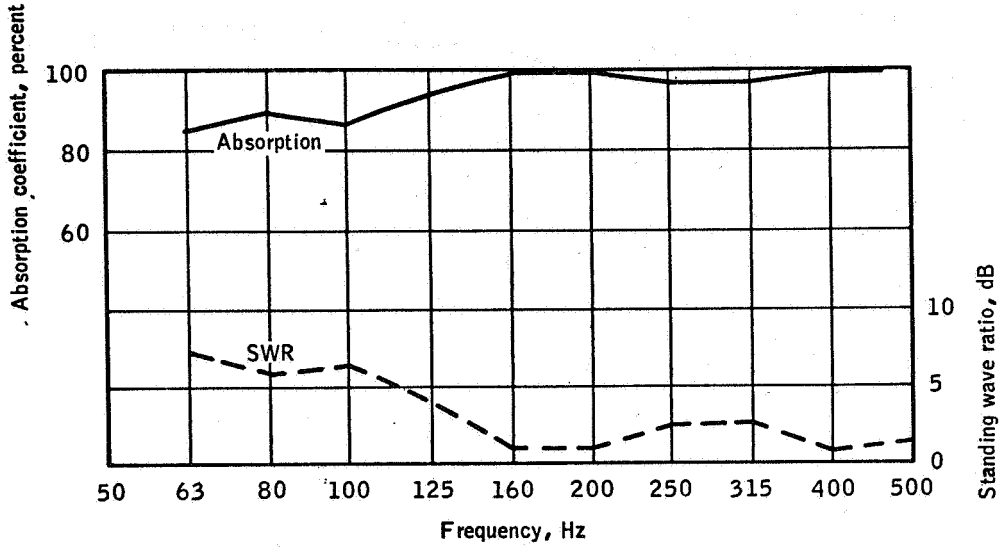

(a) Initial horn.

NASA-S-68-1044

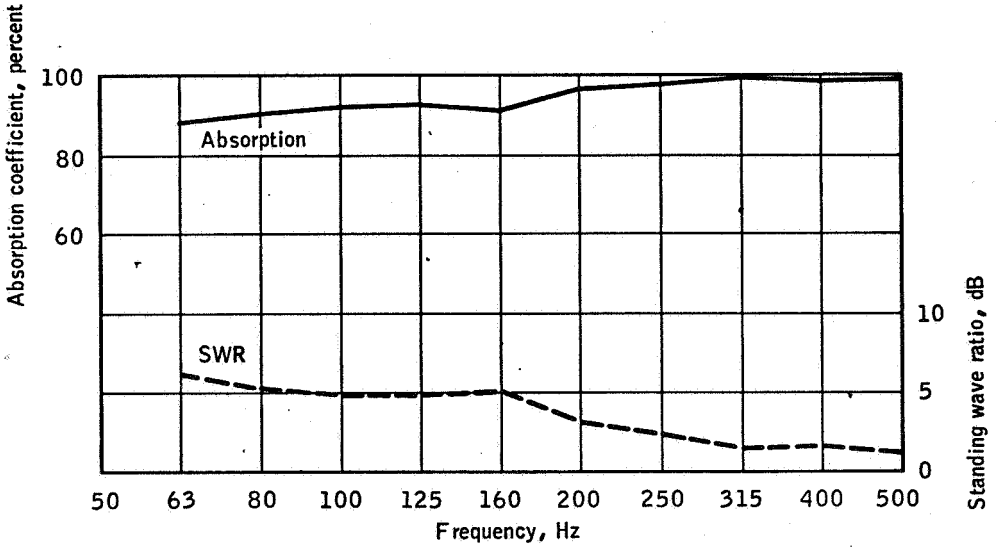

(b) Reverse horn.

Figure 26. - Typical horn characteristics.

NASA-S-68-1057

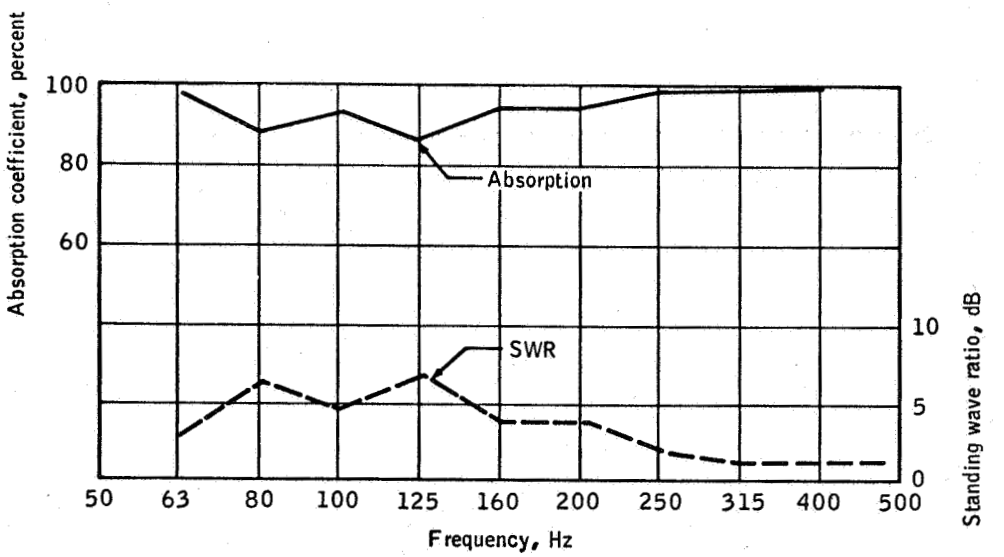

(c) Reverberant flare.

Figure 26. - Concluded.

NASA-S-68-1058

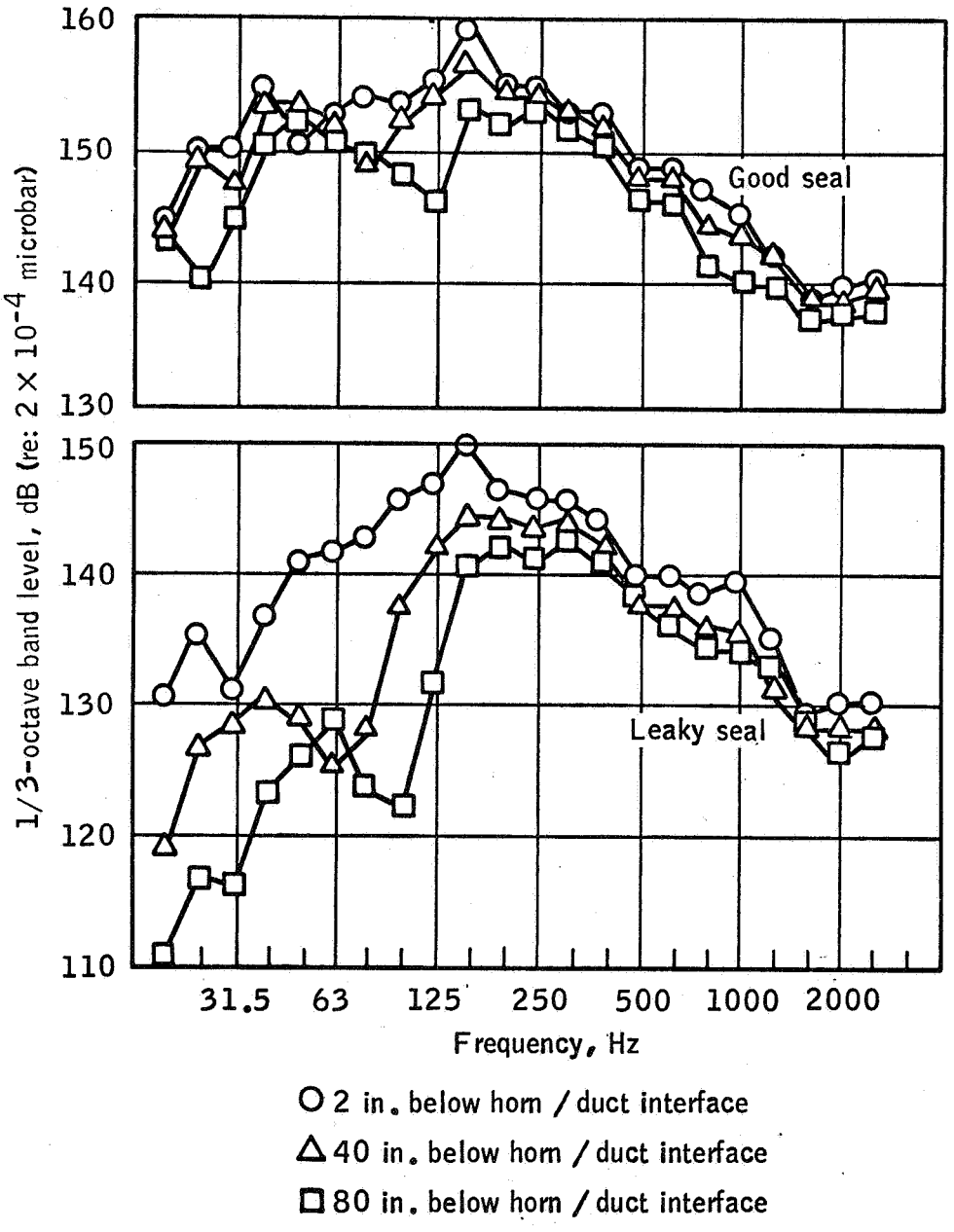

Figure 27. - Effect of seal on acoustic performance of a duct (taken from a one-third scale model).

NASA-S-68-1059

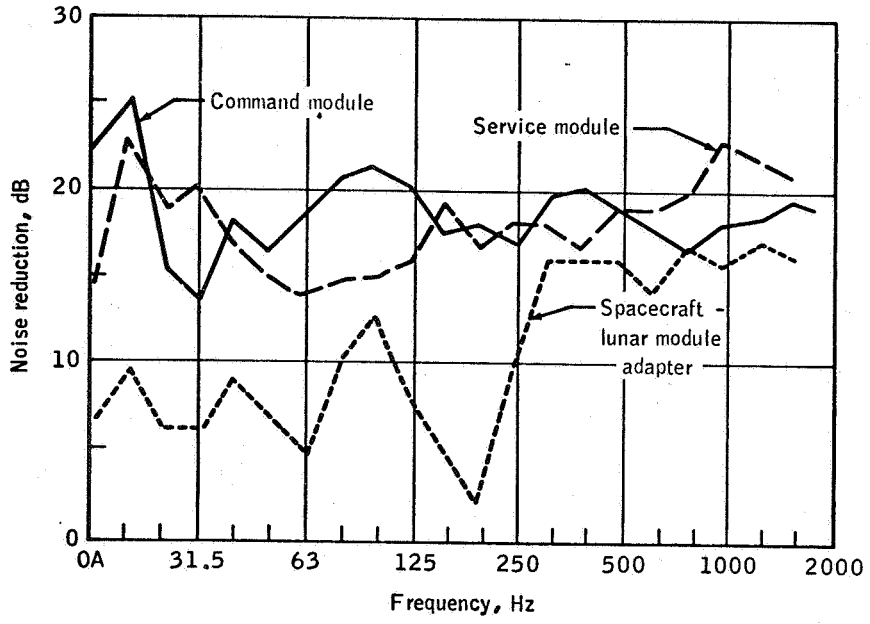

Figure 28. - Typical noise reduction between adjacent ducts.

NASA-S-68-1060

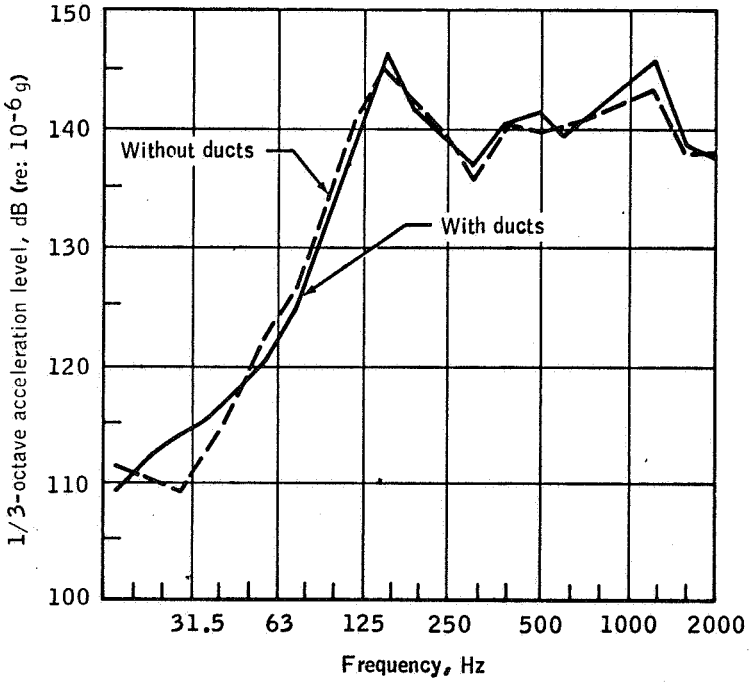

Figure 29. - Typical response of boilerplate 1150 CM with and without ducts installed.

NASA-S-68-1061

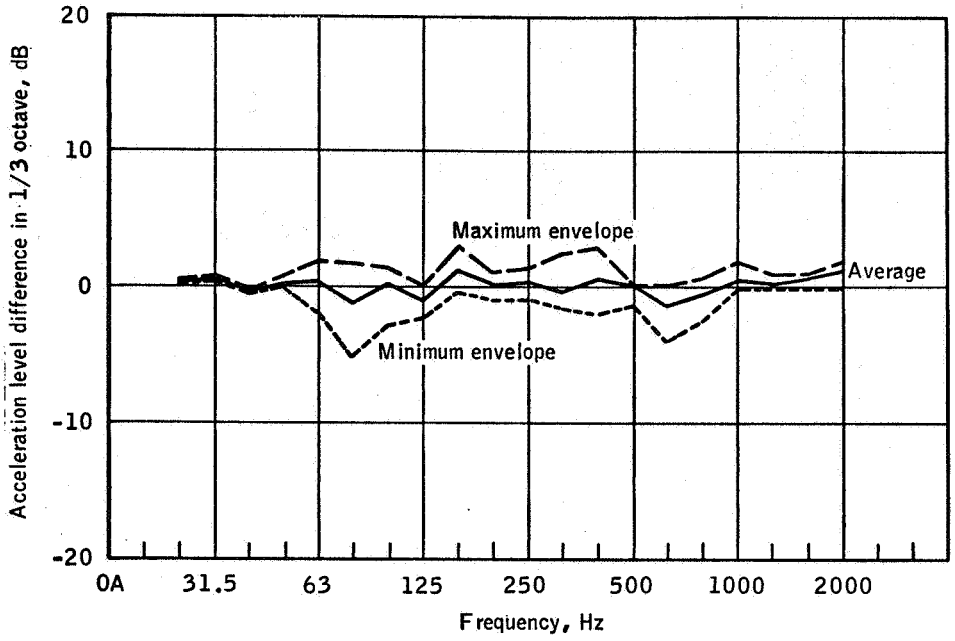

Figure 30. - Difference in airframe SLA response with and without ducts installed for six measurement locations.

NASA-S-68-1062

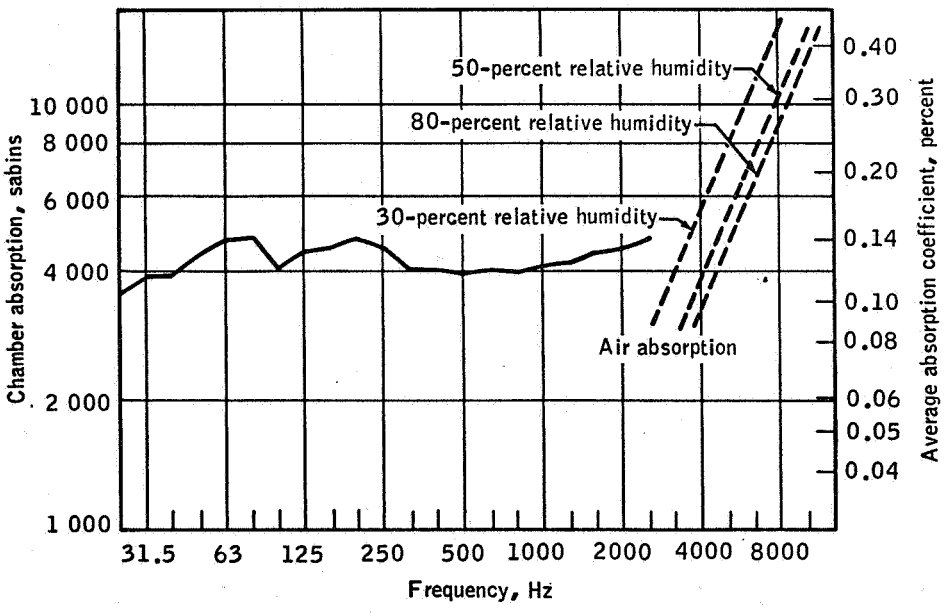

Figure 31. - SAL chamber absorption.

NASA-S-68-1063

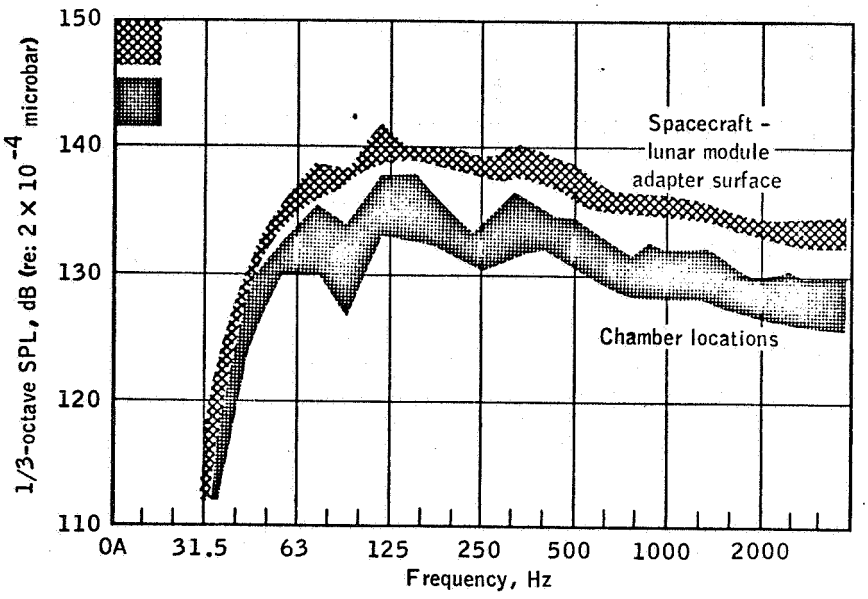

Figure 32. - Range of sound pressure spectra for SAL reverberant flare operation.

NASA-S-68-1045

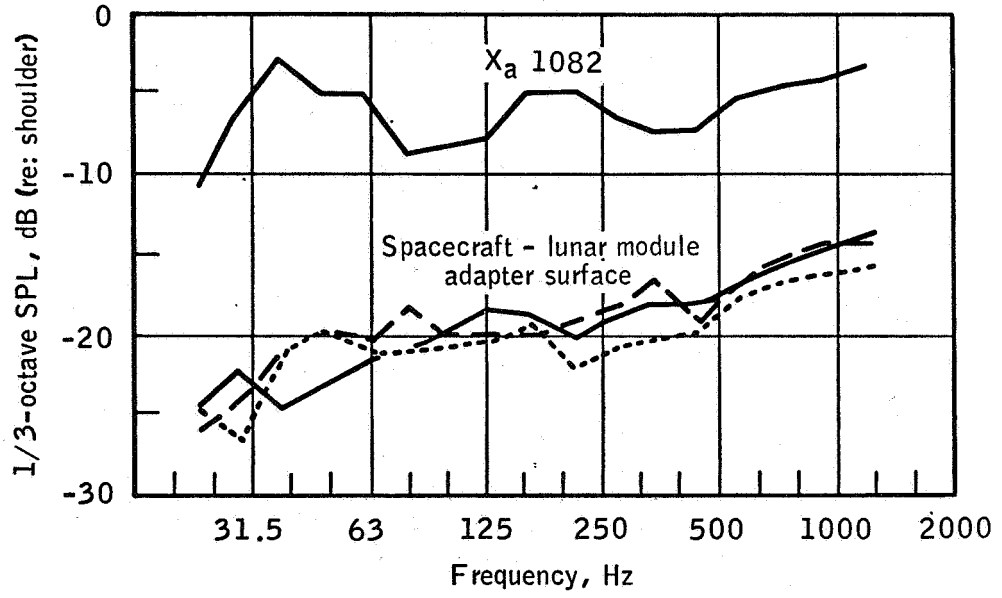

Figure 33. - Sound pressure spectra for SAL reverberant flare operation.

NASA-S-68-1046

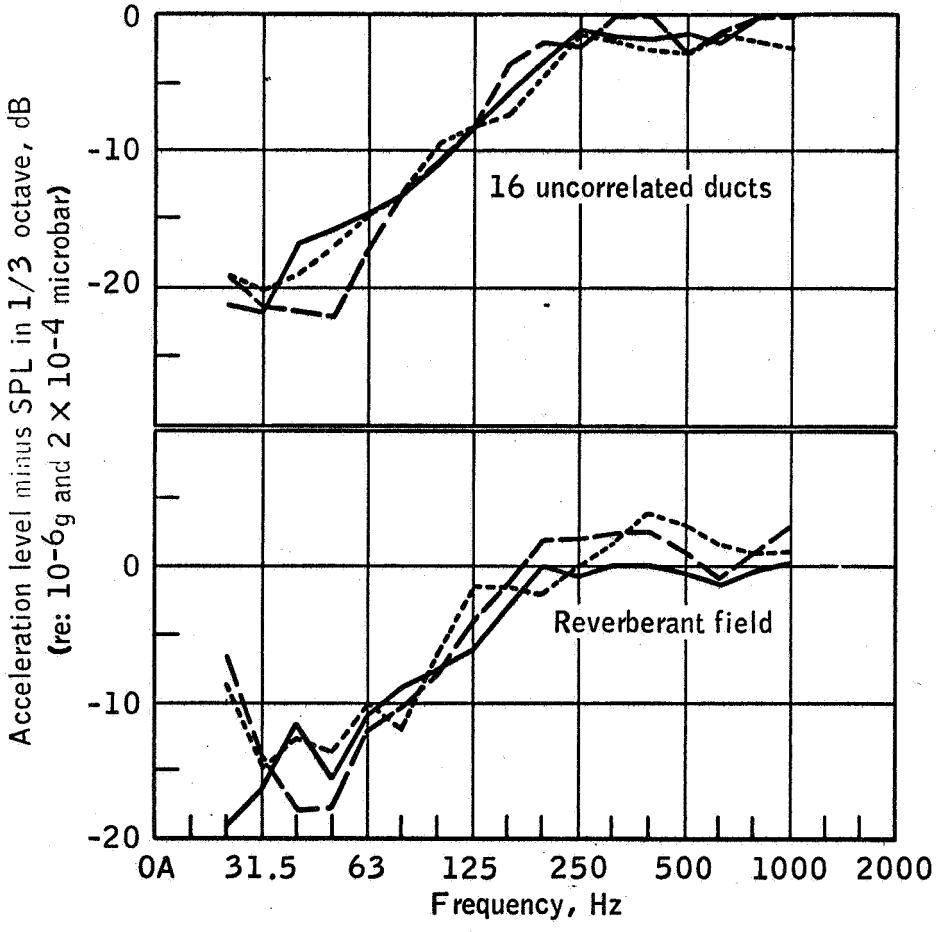

Figure 34. - SLA response characteristics at three locations for two acoustic fields.

NASA-S-68-1047

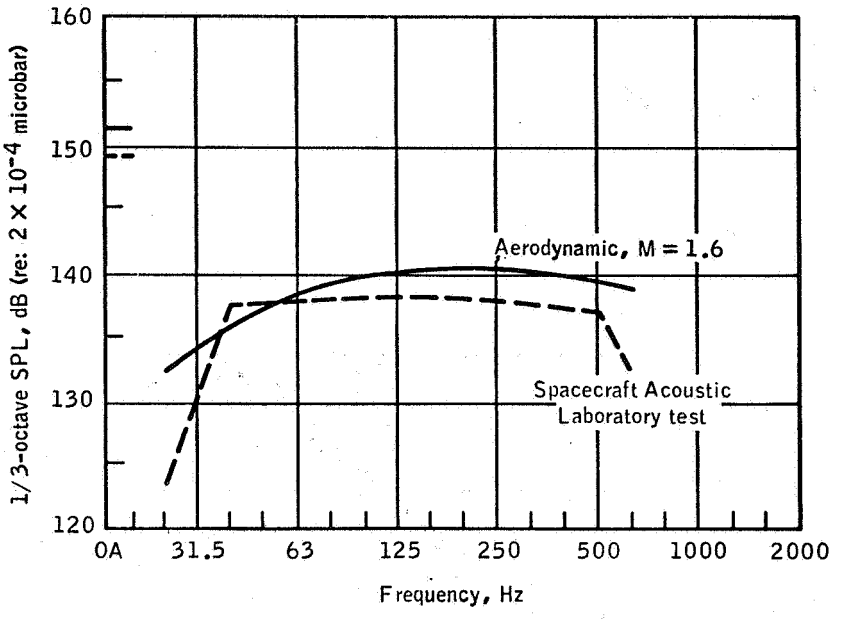

Figure 35. - Space average pressure spectra on Apollo SM.

NASA-S-68-1048

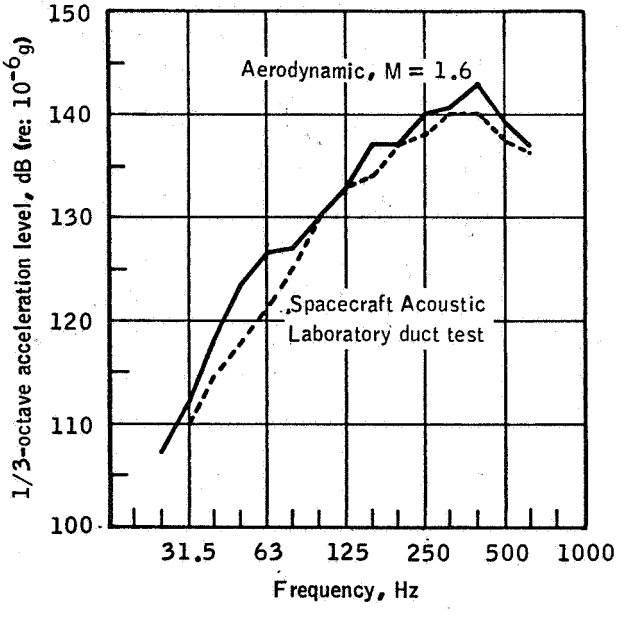

Figure 36. - Average vibration response of Apollo SM for flight and SAL pressure fields.

REFERENCES

1. Eldred, K. McK.: Concept Study for Simulation of Fluctuating Pressure Loads on the Apollo Vehicle in the Acoustic Laboratory. Rep. WR 63-11, Wyle Laboratories, Sept. 24, 1963.

2. Murray, F. M.: Acoustical Consulting Relative to the Acoustical Laboratory, Building 49, NASA Manned Spacecraft Center at Clear Lake. Rep. WR 64-6, Wyle Laboratories, Oct. 12, 1964.

3. Jones, G. W., Jr.; and Foughner, J. T., Jr.: Investigation of Buffet Pressures on Models of Large Manned Launch Vehicle Configurations. NASA TN D-1633, 1963.

4. Eldred, K. McK.: Basic Considerations in the Development of Vibro-Acoustic Test Methodology for the MSC Spacecraft Acoustic Laboratory. Rep. WR 66-33, Wyle Laboratories, June 1966.

5. White, R. W.: Predicted Vibration Responses of Apollo Structure and Effects of Pressure Correlation Lengths on Response. Rep. WR 67-4, Wyle Laboratories, Mar. 1967.

6. Dorland, W. D.; Wren, R. J.; and Eldred, K. McK.: Development of Acoustic Test Conditions for Apollo Lunar Module Flight Qualification. NASA TM X-58016, 1968.

7. Anon.: Model EPT-200 Electro-Pneumatic Transducer Instruction Manual. Rep. EPT-200-85-1, Ling Electronics, 1965.